Fermilab FERMILAB-Pub-00/364-A November 2002

Identification of A-colored Stars and Structure in the Halo of the Milky Way from SDSS Commissioning Data[1]

Brian Yanny[2,17], Heidi Jo Newberg[3,17], Steve Kent[2], Sally A. Laurent-Muehleisen[4], Jeffrey R. Pier[5], Gordon T. Richards[6], Chris Stoughton[2], John E. Anderson, Jr.[2], James Annis[2], J. Brinkmann[7], Bing Chen[8], István Csabai[9], Mamoru Doi[10], Masataka Fukugita[11,12], G. S. Hennessy[13], Željko Ivezić[14], G. R. Knapp[14], Robert Lupton[14], Jeffrey A. Munn[5], Thomas Nash[2], Constance M. Rockosi[6], Donald P. Schneider[15], J. Allyn Smith[16], Donald G. York[6]

ABSTRACT

A sample of 4208 objects with magnitude $15 < g^* < 22$ and colors of main sequence A stars have been selected from 370 square degrees of Sloan Digital Sky Survey (SDSS) commissioning observations. The data is from two long, narrow stripes, each with an opening angle of greater than 60°, at Galactic latitudes $36° < |b| < 63°$ on

[1]Based on observations obtained with the Sloan Digital Sky Survey, and with the Apache Point Observatory 3.5-meter telescope, which is owned and operated by the Astrophysical Research Consortium

[2]Fermi Accelerator National Laboratory, P.O. Box 500, Batavia, IL 60510

[3]Dept. of Physics, Applied Physics and Astronomy, Rensselaer Polytechnic Institute Troy, NY 12180

[4]LLNL/IGPP 7000 East Ave., L-413, Livermore, CA 94550

[5]U.S. Naval Observatory, Flagstaff Station, P.O. Box 1149, Flagstaff, AZ 86002-1149

[6]University of Chicago, Astronomy & Astrophysics Center, 5640 S. Ellis Ave., Chicago, IL 60637

[7]Apache Point Observatory, P.O. Box 59, Sunspot, NM 88349-0059

[8]Department of Physics and Astronomy, The Johns Hopkins University, 3701 San Martin Drive, Baltimore, MD 21218, USA

[9]Department of Physics of Complex Systems, Eötvös University, Pázmány Péter sétány 1/A, Budapest, H-1117, Hungary

[10]Department of Astronomy and Research Center for the Early Universe, School of Science, University of Tokyo, Hongo, Bunkyo, Tokyo, 113-0033 Japan

[11]Institute for Cosmic Ray Research, University of Tokyo, Midori, Tanashi, Tokyo 188-8502, Japan

[12]Institute for Advanced Study, Olden Lane, Princeton, NJ 08540

[13]U.S. Naval Observatory, 3450 Massachusetts Ave., NW, Washington, DC 20392-5420

[14]Princeton University Observatory, Princeton, NJ 08544

[15]Department of Astronomy and Astrophysics, The Pennsylvania State University, University Park, PA 16802

[16]University of Michigan, Department of Physics, 500 East University, Ann Arbor, MI 48109

[17]Equal first authors

the celestial equator. Relative photometric calibrations good to 2% and consistent absolute photometry allows this uniform sample to be treated statistically over the large area. An examination of the sample's distribution shows that these stars trace considerable substructure in the halo. Large overdensities of A-colored stars in the North at $(l, b, R) = (350, 50, 46\,\mathrm{kpc})$ and in the South at $(157, -58, 33\,\mathrm{kpc})$ and extending over tens of degrees are present in the halo of the Milky Way. Ivezic et al. (2000) has detected the northern structure from a sample of RR Lyraes in the SDSS.

Using photometry to separate the stars by surface gravity, both structures are shown to contain a sequence of low surface gravity stars consistent with identification as a blue horizontal branch (BHB). Both structures also contain a population of high surface gravity stars two magnitudes fainter than the BHB stars, consistent with their identification as blue stragglers (BSs). The majority of the high surface gravity stars in the Galactic halo may be blue straggler stars like these. A population of F stars associated with the A star excess in the southern structure is detected (the F stars in the northern structure at 46 kpc would be too faint for the SDSS to detect). From the numbers of detected BHB stars, lower limits to the implied mass of the structures are $6 \times 10^6 M_\odot$ and $2 \times 10^6 M_\odot$, though one does not yet know the full spatial extent of the structures. The fact that two such large clumps have been detected in a survey of only 1% of the sky indicates that such structures are not uncommon in the halo.

Simple spheroidal parameters are fit to a complete sample of the remaining unclumped BHB stars and yield (at $r < 40$ kpc) a fit to a halo distribution with flattening $(c/a = 0.65 \pm 0.2)$ and a density falloff exponent of $\alpha = -3.2 \pm 0.3$.

Subject headings: Galaxy: structure — Galaxy: halo — stars: early-type — blue stragglers — horizontal branch

1. INTRODUCTION

1.1. Halo structure

Observations of distinct populations of stars in the Milky Way Galaxy (young, metal-rich stars in the disk and older, metal-poor stars in the halo) led Eggen, Lynden-Bell, & Sandage (1962, ELS) to propose that the Galactic halo formed before the disk, during the rapid collapse of a gas cloud. In this picture, the stars in the halo are approximately the same age, with abundances which increase towards the center of the Galaxy. The model predicts a relatively smooth form and shape for the halo. Simple models, for instance, parameterize the distribution of matter in the Galactic halo as a flattened spheroid, where the flattening is given by an axial ratio $c/a \leq 1$ (and $b/a \leq 1$ if triaxiality is considered), with a power-law density profile $\rho(r) \sim r^\alpha$.

As the positions and motions of luminous objects in the Galactic halo in principle provide tracers of mass within the halo potential, study of these objects is important for understanding the

distribution of dark matter as well as providing clues to the formation of the Galaxy.

Model parameters for this simple description of the halo have been obtained by empirical fits to the distributions of such astronomical objects as Galactic globular clusters, K dwarfs, and A-colored stars. Here the term "A-colored stars" includes all types of stars, including blue horizontal branch (BHB) and blue straggler (BS) stars, which have colors and spectra similar to those of the bright, nearby, main sequence A stars on which the spectral classification was defined. The distribution of Galactic globular clusters yields a fit to the structure parameters of $c/a \sim 1$ and $\alpha \sim -3.5$ (Harris 1976; Zinn 1985). Saha (1985) used RR Lyrae stars to find $\alpha \sim -3$ out to distances of 25 kpc, with a steeper decline thereafter. Ivezic et al. (2000) also measured a distribution of RR Lyrae stars with $\alpha \sim -3$ to at least 50 kpc. Hubble Space Telescope counts of K dwarfs by Gould, Flynn, & Bahcall (1998) yield $c/a = 0.8 \pm 0.1$, and $\alpha = -3.06 \pm 0.22$.

It is of course not required that c/a remain constant with Galactocentric radius. Preston, Shectman, and Beers (1991) counted BHB stars and found evidence that c/a increases from 0.5 to 1 as one moves out to $R > 20$ kpc with $\alpha = -3.5$. Using this changing c/a, Wetterer & MacGraw (1996) find $\alpha = -3.53 \pm 0.077$ for RR Lyraes. Sluis & Arnold (1998) find a flat c/a, but less evidence for changing flattening with Galactocentric radius. As part of an extensive kinematic analysis of several hundred nearby halo stars with [Fe/H] ≤ -1.8, Chiba and Beers (2000) find that the axial ratio increases from 0.65 at $R < 15$ kpc to 1.0 at $R \sim 20$ kpc. Most of these studies use a few hundred objects at most on which to base their results, and only a few, such as Chiba and Beers (2000), have kinematic information.

In contrast to the ELS model, recent research suggests that some or all of the halo may have been formed through accretion of smaller dwarf galaxies (see Johnston et al. 1999; Majewski 1999, and references therein). One example of a dwarf galaxy thought to be in the process of accreting has been discussed by Ibata, Gilmore, and Irwin (1995). As these smaller galaxies fall into the Milky Way, they may be tidally disrupted and break up into long streams of stars which can persist for 1-10 Gyr (Lynden-Bell & Lynden-Bell 1995; Johnston 1998; Helmi et al. 1999).

1.2. The nature of A-colored stars in the Galactic halo

A-colored stars at faint magnitudes are usually assumed to be halo population (Pop II) stars, and hence BHB stars. However, it has become clear that many distant blue stellar objects have hydrogen line widths indicative of main sequence gravity A stars rather than the less massive BHB stars (Rodgers, Harding, and Sadler 1981; Sommer-Larsen, Christensen & Carter 1989; Beers et al. 1992; Preston, Beers, and Shectman 1994; Wilhelm et al. 1999).

Why can't all of these high-gravity A-colored stars be normal main-sequence stars? The well-known arguments against this are two-fold: First, except for dwarf irregular companions to the Milky Way such as the LMC and the Sextans dwarf, there is no evidence that significant star formation has taken place in the far halo (R > 30 kpc) within the last billion years, which is

greater than the main-sequence lifetime of an A star. Second, the stars are too far from the star forming regions in the Galactic plane to have reached their present positions in the far halo with any reasonable assumed velocity (it takes 300 Myr to travel 30 kpc at 100 km s^{-1}).

Blue straggler stars in globular clusters, which have ages closer to 10 Gyr, are an interesting example of high surface gravity A-colored objects which are present in an old environment. These high surface gravity BS stars are generally thought to be main sequence stars which result from mergers of, or mass transfer between, two lower mass stars (Stryker 1993; Sills & Bailyn 1999). Whatever their formation mechanism, they should also be present at some level in the field of the Galactic halo (Rodgers and Roberts 1993; Norris and Hawkins 1991).

1.3. The Sloan Digital Sky Survey

The Sloan Digital Sky Survey (SDSS) is a large, international collaboration set up to survey 10,000 square degrees of sky in five optical passbands and to obtain spectra of a million galaxies, one hundred thousand quasars, and tens of thousands of Galactic stars. The data are being taken with a dedicated 2.5 meter telescope located at Apache Point Observatory (APO) near Cloudcroft, New Mexico. The telescope has two instruments: a CCD camera with 30 2K x 2K CCDs in the focal plane, and two 320-fiber double spectrographs. The imaging data are tied to a network of brighter astrometric standards (which would be saturated in the main imaging data) through a set of twenty-two smaller CCDs in the focal plane of the imaging camera. A 0.5 m telescope at APO will be used to tie the imaging data to brighter photometric standards.

The USNO 1m telescope at Flagstaff, AZ, has been used to define the photometric system, defining SDSS standard stars in u', g', r', i', and z' (Smith et al., in preparation). Since the precise calibration for the SDSS filter system is still in progress, magnitudes in this paper are quoted in the $u^*g^*r^*i^*z^*$ system, which approximates the final SDSS system. These systems differ absolutely (with negligible color terms) by only a few percent in $g^*r^*i^*z^*$, and no more than 10% in u^*. See York et al. (2000), Fukugita et al. (1996) and Gunn et al. (1998) for further information on the SDSS, the filter system and the imaging camera.

The SDSS has imaged a large fraction of the celestial equator ($-1.25° < \delta < 1.25°$) as part of telescope and imaging camera commissioning. Catalogs produced from nearly 400 square degrees of these data contain thousands of A-colored stars suitable for probing the halo, with absolute photometry good to $\sim 5\%$ for objects with $g^* < 20$. For reference, blue stars with $0 < B - V < 0.2$ (including A stars), have a SDSS g^* magnitude approximately equal to their Johnson V magnitude.

2. THE SAMPLE OF A-COLORED STARS

2.1. Photometric Observations and Data Samples

The SDSS camera contains six columns of CCDs, each of which records data for a 0.23 degree wide strip of the sky. The CCDs are continuously read out as the camera scans a great circle across the sky at the sidereal rate, so the length of an imaged strip grows at 15 degrees per hour. The effective exposure time in each of the 5 filters is 54 seconds. A "run" generates six parallel continuous strips of sky with a gap of 0.2 degrees between columns. A second "run," offset slightly from the first, is obtained to fill in the sky between the first six scan lines and fully image a 2.5 degree wide "stripe" on the sky.

Figure 1 shows $u^* - g^*$ vs. $g^* - r^*$ for all stellar objects with $g^* < 21$ in 13.3 square degrees of one column of SDSS data. Objects in different magnitude ranges are plotted in different colors. As discussed by Newberg et al. (1999), the position of the blue end of the Galactic stellar locus shifts as a function of magnitude due to the sampling of populations of stars with different characteristic metalicities at different scale heights in the disk. The temperatures as a function of color can be estimated by comparison with Lenz et al. (1998). The stars in the A box in the diagram are expected to contain nearly exclusively hot stars with a strong Balmer jump – BHB stars, BSs, and main sequence stars with spectral type A. These bluer objects do not shift by large amounts in color with magnitude. Boxes for quasar candidates, F, and G type stars are also indicated and will be discussed below.

All of the magnitudes used in this paper are point spread function (PSF) fitted magnitudes for stellar objects, generated by summing the PSF-weighted flux for each object (Lupton et al., in preparation). Saturation sets in for A-colored objects brighter than $g^* \sim 15$. All magnitudes in this paper use the modified flux designation for faint magnitudes described in Lupton, Gunn, & Szalay (1999), though for the range of magnitudes relevant here, $15 < g^* < 22.5$, the distinction is negligible.

The boundaries of the A-colored star box were chosen to provide a sample of A stars, BHBs and BSs, free from contamination from other populations of objects even to magnitudes as faint as $g^* \sim 21$. The choice of a $g^* - r^* = 0$ red limit was conservatively chosen in order to ensure that the Gaussian tail of color measurement errors of the population of the very large numbers of F stars did not begin to scatter into the A star box at faint magnitudes.

All magnitudes and colors in the present work have been corrected for reddening using the maps of Schlegel, Finkbeiner & Davis (1998). Since all of the A-colored objects sampled here are at distances d >> 1 kpc from the plane of the Galactic disk, where most reddening-producing dust occurs, the full reddening correction of Schlegel, Finkbeiner & Davis (1998) is applied to all objects.

For this analysis, two samples of A-colored stars are chosen from two stripes of data. The northern sample (north of the Galactic plane on the celestial equator) is a filled stripe from SDSS

runs 752 and 756, obtained 1999 March 21 and 22. The stripe is 87 degrees long ($145.5° < \alpha < 232.5°$ [J2000], and 2.52 degrees wide ($-1.26° < \delta < 1.26°$), with 219 square degrees of data. Data in the region $215.5° < \alpha < 216°$ from run 752 was excluded, since the seeing increased sharply to $3''$ in this region (compared to typical seeing of $1.3''$ for the rest of the scan). In Galactic coordinates, the northern sample runs in a long arc from [l,b] = [236,37] up to [303, 63] and then gradually back to [4, 43].

The northern sample contains 3126 point sources (extended sources are rejected) in the runs 752 and 756 which have dereddened colors in the box in Figure 1 ($0.8 < u^* - g^* < 1.5$ and $-0.3 < g^* - r^* < 0.0$), and which have u^* errors smaller than 30% (corresponding to a limit of $g^* \sim 22.5$).

The southern sample (south of the Galactic plane on the celestial equator) is a filled stripe from SDSS runs 94 and 125, obtained 1998 September 19 and 25. The stripe is 60 degrees long ($353° < \alpha < 53°$) and 2.5 degrees wide ($-1.24° < \delta < 1.27°$), with 151 square degrees of data. The southern sample contains 1082 stars, to $g^* \sim 22$, with the same selection criteria as the northern sample. The southern sample runs from [l,b] = [85,-57] through [125,-63] and then back to [184,-43].

The SDSS has imaged the majority of these equatorial regions twice. SDSS runs 259, 273 and 745 (obtained 1998 November 17, 19 and 1999 March 20, respectively), nearly completely overlap runs 94, 125 and 756, and are used to verify the findings in the primary runs.

The list of A-colored stars from runs 745 and 756 were matched (without the requirement that the error in u^* be smaller than 30%), based on position (within one arcsecond, well in excess of typical one sigma astrometric errors of 100 mas). Additionally, objects from these overlapping scans were matched without regard to color in order to estimate completeness, detection limits and reproducibility of the data. The upper curve in Figure 2 shows the fraction of objects matched as a function of g^* for all stellar sources. The lower and noisier curve is that for matched objects within the A-colored box only. The maximum level of $\sim 80\%$ matched in the lower curve is primarily due to objects in one sample or the other scattering out of the box. One can estimate this fraction by noting that most of the objects in the box are on the red side, giving the box an effective width of 0.15 mag in $g^* - r^*$. When combined with typical color errors of 2% for two measurements, one derives an expected fraction $f = 1 - 0.02 * \sqrt{2}/0.15 = 81\%$. The matched fraction decreases rapidly for $g^* > 20.0$. Here, the requirement that the object fall within the box in $u^* - g^*$ becomes the determining factor. From Figure 2, one sees that the A-colored star sample is uniform (in the sense that it samples the same population of stars) to $g^* \sim 20$ and has detections to about $g^* \sim 22.5$ (50% limit) in the northern stripe. After $g^* \sim 20$ the population of stars includes an increasing fraction of stars slightly redward of the box whose photometric errors have scattered them into the box. The fact that the upper curve doesn't start to drop until $g^* \sim 22.5$ indicates that the uniform sample is not affected by the detection limit, and is in that sense complete. A related procedure in the south yields a uniform sample to $g^* = 19.5$ and detections to $g^* \sim 22$.

2.2. Distribution of the A-colored stars

Horizontal branch stars, especially those in a restricted color range, are approximately standard candles. A BHB absolute magnitude of $M_{g^*} = +0.7$ can be used to infer approximate heliocentric distances from magnitudes for these objects. This absolute magnitude was calculated by converting the V absolute magnitude of halo RR Lyrae stars from Layden et al. (1996) into the g^* filter, using the transformations from Fukugita et al. (1996) for the colors of RR Lyrae stars. Since the g^* magnitudes of RR Lyrae stars in Pal 5 (Figure 7) are similar to the BHB magnitudes in Pal 5, the assumption has been made throughout this paper that the absolute magnitudes of BHBs are the same. This approximation is dependent on the blue response of the filter used. Note, for example, that Preston, Shectman, and Beers (1991), find that for objects with colors at the blue end of the A star selection box, BHBs are about 0.9 magnitudes fainter in V than the RR Lyrae magnitude (this corresponds to a difference of 0.7 magnitudes in g^*, given the transformations in Fukugita et al. 1996).

Figure 3 presents a wedge diagram with Right Ascension and g^* magnitude for all 4208 A-colored stars from both North and South samples. Significant structures are immediately apparent. The clump at [l,b] = [242,43], or $(\alpha, \delta) = (153, 0)$, and $20.50 < g^* < 20.55$ is the northern half of the Sextans dwarf irregular galaxy (van Dyk, Puche, & Wong 1998) at $d = 70$ kpc (the southern half of Sextans is at $\delta < -1.25°$ and is not covered in this data set). One also notes two dramatic arcs of structure at $g^* \sim 19$ and $g^* \sim 21$ in the North ($195° < \alpha < 230°$), and similar, though less pronounced, structure at $g^* = 18$ and $g^* \sim 20$ in the South ($20° < \mathrm{RA} < 45°$).

The large structure in the north was detected by Ivezic et al. (2000) in a search for variable RR Lyrae stars in the overlapping SDSS runs 745 and 756 taken two days apart. It contains a remarkable population of ~ 80 RR Lyraes clustered in the same way as the bluer A-colored stars in the northern sample.

There are numerous smaller apparent concentrations throughout this diagram. The Galactic globular cluster, Pal 5, for example, has its horizontal branch at $g^* = 17.3$, $\alpha = 229°$ in the North. An enlargement of the three degrees of arc in the Pal 5 area of sky is shown to the right in Figure 3. Along with the stars of Pal 5's BHB at $g^* = 17.3$, the narrow sequence of Pal 5 BSs (see §4.1) is clearly visible from $18.5 < g^* < 20$, also at $\alpha = 229°$.

2.3. Verification of the Halo Substructure

A number of straight-forward checks are performed to verify that the large structures in Figure 3 are not artifacts.

In order to assess whether these structures could be due to selection effects, low-redshift quasar candidates are color selected from the SDSS survey from a color box with boundaries $-0.05 < u^* - g^* < 0.15$, $-0.1 < g^* - r^* < 0.0$ (the small Q box in Figure 1) and plotted in Figure 4.

Figure 4 shows no significant magnitude (and thus implied spatial) structure to $g^* \sim 22$, except for the increasing density of quasar candidates to fainter magnitudes. While not every object in this color box is a quasar, other hot blue sources which contaminate the low redshift quasar population, such as white dwarfs and narrow emission line compact galaxies, also have population distributions which are expected to be isotropic, showing no structural signature of the Galactic disk, bulge or halo (Fan et al. 2000). The uniformity of the distribution in Figure 4 demonstrates the uniformity of the photometry and calibration in the SDSS samples to magnitude limits of $g^* \sim 22$ for objects with colors similar to A stars. Fainter than $g^* \sim 22$, the errors in the u^* magnitudes of F stars become large enough that some of them scatter into the quasar color box. The distribution of F stars in the northern and southern sample areas is discussed in §4.5.

The photometric calibration within an individual stripe is accurate to a few percent due to the continuous drift scanning-method of data collection and photometric observing conditions. Relative photometric accuracy of objects detected in multiple scans is good to $\sim 2\%$ for blue objects to $g^* \sim 20$ in the $g^*r^*i^*$ and z^* filters. The absolute calibration, and the calibration between runs observed in different seasons, relies upon calibration patches obtained with a small photometric telescope, and is not yet final.

To verify that the absolute calibration is essentially identical in the northern and southern stripes, the density of quasar candidates (chosen from the larger Q box in Figure 1 to increase statistics) as a function of magnitude for the North and South is plotted in Figure 5. The excellent agreement between the two data sets to $g^* \sim 21.5$ is further evidence that the photometric calibration is uniform across the sky. One notes from the earlier falloff for southern quasar candidates in Figure 5 that the southern sample completeness limit is about 0.5 magnitudes brighter than that of the northern sample. As the objects are selected in the bluest SDSS filters, and since the u' filter is the least sensitive filter, completeness limits and the magnitude limit for detections of objects in the present work is determined primarily by where the error in the u^* band flux for objects becomes large. Note that although $g^* - r^*$ colors for quasars and A stars are similar, the $u^* - g^*$ colors of quasars are bluer than A stars by about one magnitude. Therefore, one expects to see a drop in A-star counts one magnitude brighter than the drop in quasar counts, as is verified by comparing the upper curve in Figure 2 to the northern points in Figure 5.

The duplicate equatorial runs 745 and 273 were used to generate a plot similar to that shown in Figure 3. The structures noted in §2.2 are also clearly visible in Figure 6, though there are fewer stars since only half of a filled stripe is plotted. Note that run 745 doesn't cover Sextans in RA, but does extend beyond the end of the northern structure, and thus more clearly defines its full length than in Figure 3.

3. SPECTROSCOPIC FOLLOW-UP

3.1. Observations

While the SDSS continues commissioning of its spectrographs, which will obtain thousands of spectra of type A and BHB stars in addition to its main galaxy and quasar redshift survey, a small number of representative spectra have been obtained with other telescopes to investigate the nature of the selected A-colored objects.

The observations produced spectra for a sample of 6 A-colored stars selected from the SDSS samples, along with spectra of 5 A-colored reference stars with known surface gravities.

The Lick Observatory 3 m telescope was used to obtain reference stars, including CS 29516-0011, a BHB identified as a field horizontal branch star by Wilhelm et al. (1999); WD 0148+467, a DA white dwarf identified by Gliese & Jahreiss (1979); and HD 13433, a known A0V star classified by Houk & Smith-Moore (1988), all with $8 < V < 12$. These spectra were obtained with exposures between 5 s and 60 s on the night of 1998 Dec 19 at a resolution of about 6Å, obtaining good S/N ratios of about 50:1 in the continua.

Figure 7 shows the color-magnitude diagram of Pal 5, generated from reddening-corrected SDSS data. Stars of all colors within ~ 9 arcminutes of the center of the globular cluster Pal 5 were selected; note that there is significant field contamination here at [l,b]=[1,46]. The vertical lines show the $g^* - r^*$ limits of the A-colored star box. A 5400 s exposure of one blue straggler and a 1800 s spectrum of a BHB star (marked with circled squares in Fig. 7) were taken at 3Å resolution with the dual imaging spectrograph (DIS) on the ARC 3.5 meter telescope at Apache Point Observatory on the night of 1999 May 11. Proper motion studies confirm that both objects are members of the Pal 5 globular cluster (K. Cudworth, private communication). The resolution of these spectra is approximately 3Å at a S/N $\sim$ 30 for the brighter object and 15 for the fainter. Wavelength calibrations were obtained and standard flats and reductions were applied to all spectral data.

Six additional 30 min spectra of $17 < g^* < 18$ A-colored stars selected from the SDSS were observed on the nights of 1999 May 8, 10, and 11 with the DIS at 3Å resolution and S/N of ~ 20. The six spectra all confirmed that the A-colored star sample indeed consists entirely of blue stars with strong Balmer lines, and is not contaminated by significant numbers of white dwarfs, quasars or other extragalactic objects such as compact E+A galaxies.

3.2. Spectroscopic Surface Gravity Indicator

The primary diagnostic used to distinguish BHBs from A main sequence (or blue straggler) stars is the widths of the Balmer line profiles as indicators of stellar surface gravity (see Pier 1983, and references therein). Main sequence A stars ($M \sim 2.5 M_\odot, R \sim 2 R_\odot$) have $3.5 < \log g < 5$, while horizontal branch stars, which have much smaller mass ($M \sim 0.7 M_\odot$) and larger radii $\sim 3 R_\odot$,

have $2.5 < \log g < 3.2$. This difference in surface gravities clearly shows up in the Stark pressure-broadened Balmer line profiles. White dwarfs, which have much higher surface gravities – typically $\log g > 7.5$, are easily distinguished from main sequence A stars. Since white dwarf $u^* - g^*$ colors are significantly bluer than those of A and BHB stars, they are not present in the A-star selection box in significant numbers. None of the spectra of A-colored stars presented here is consistent with a white dwarf identification.

The standard indicator which separates main sequence gravity A stars from lower surface gravity BHB stars is the width of the Hδ line at 80% of the continuum. One typically uses the Hδ line because the A star flux is higher here than in longer wavelength Balmer lines, and it is easier to fit the continuum at Hδ than at shorter wavelength Balmer lines. The width at 80% of the continuum is a measurement robust to the presence of metal lines which can apparently widen the absorption lines near the continuum, and is insensitive to a range of instrumental resolutions, which can change the measured depth of the line.

IRAF was used to extract the 1D spectra, select a region of the spectrum containing the Hδ and Hγ lines, divide the continuum by a best fit 6th order Legendre polynomial, and then boxcar smooth and wavelength shift the spectra to match the resolution and redshift of the Lick reference spectra. The difference in resolution between the sets of observations is not critical, since the broad Balmer lines typically have equivalent widths of 30Å. It must be noted that with very wide Balmer lines it is difficult to uniformly fit the continuum in such a way that the lines themselves do not affect the fit.

The results are plotted in Figures 8-9. Figure 8 shows the Pal 5 stars compared to the blue reference templates. The BHB star in Pal 5 is a good match to the template BHB star. The spectrum of the Pal 5 blue straggler has much larger line widths consistent with the template A0V star. The six additional representative A-colored objects were spectroscopically confirmed with spectra shown in Figure 9. For these six brighter ($17 < g^* < 18$) SDSS northern sample targets observed from APO in Figure 9, 4 have narrow widths, one has a broad width (lower left panel), and one is apparently a metallic-lined Am star (upper left panel).

Table 1 summarizes the spectroscopic targets, listing SDSS id (or other id such as HD number), α, δ , dereddened g^* magnitude, $u^* - g^*$, $g^* - r^*$, $H_\delta(0.8)$, l, b, and classification determined from the Balmer line widths in the spectrum.

The radial velocities of the stars were only approximately measured (with typical error of 30 km s^{-1}), and ranged from -120 to +120 km s^{-1}, consistent with halo objects. The resolution of the observations and uncertainties in the wavelength calibrations made it difficult to draw conclusions about clustering of this small sample of objects from radial velocities. Kinematic information will of course be an important future diagnostic of SDSS A-colored stars in continuing searches for coherent halo structures.

4. THE NATURE OF THE A-COLORED STAR SAMPLE

4.1. The Example of Pal 5

As previous authors (Preston, Shectman, and Beers 1991; Norris and Hawkins 1991; Preston, Beers, and Shectman 1994; Wilhelm et al. 1999) have noted, and the spectroscopy in this paper also shows, one must be careful drawing conclusions about Galactic structure from color-selected A-stars in the halo of the Milky Way, since the blue star population is not homogeneous; it includes at least two types of objects.

One gains insight into the nature of the A-star sample by examining the appearance of the globular cluster Pal 5 in the star distribution in Figure 3 at $\alpha = 229°$. Pal 5, located about 20 kpc from the Sun, contributes 5 BHB stars at $g^* \sim 17.3$, and at least 7 BS stars at $18.5 < g^* < 20.0$ (see Figure 7). On an absolute scale, the BHBs in Pal 5 have $M_{g^*} \sim 0.7$, and the BSs are thus at absolute magnitudes of $1.9 < M_{g^*} < 3.4$.

The large parallel arcs of A-colored stars present in Figure 3 are also separated by about 2 magnitudes, suggesting that they might represent associated BHB and blue straggler stars at a common distance. If this assumption is correct, then one can use the location of the BHB in g^* and the absolute magnitude of BHB stars to determine a distance to the stars in the arcs. For example, the northern arc, with an implied BHB magnitude of $g^* \sim 19$, is then approximately 45 kpc from the Sun.

4.2. Photometric determination of surface gravity

In order to support the identification of the stars in the overdensities, one would like to be able to separate all of the high surface gravity stars from the low surface gravity stars. Presently lacking individual spectra for such a large sample, one turns to photometric multi-color indicators of surface gravity in the SDSS filters. From a sample of 1121 A-colored stars, Wilhelm et al. (1999) show that they can separate (although not perfectly) high surface gravity stars from low surface gravity stars in $U-B, B-V$ color-color diagrams. Due to the lack of a single-valued transformation between the U and u^* (they have different behavior around the Balmer jump), a simple conversion between $u^* - g^*$ and $U - B$ is not well defined. Thus, although one cannot precisely convert the $U - B, B - V$ color separation criteria to the SDSS filter system, a similar idea is applied to approximately separate the populations: extreme Balmer jump BHB stars are in general slightly bluer in $g^* - r^*$ and redder in $u^* - g^*$ than those with higher gravities.

The other SDSS filters available (i^*, z^*) may be considered for color separation of gravities. For instance, Lenz et al. (1998) show that in synthetic A stars derived from Kurucz model spectra Kurucz (1991), different gravities separate well in the z' filter, and they derive a direction in SDSS color space that results in maximum separation. Since z^* magnitudes accurate to 2% are lacking, for most of the faint A star sample considered here, the stars were separated in $u^* - g^*$ and $g^* - r^*$

only. (The $r^* - i^*$ color contributes little to surface gravity separation for objects with A star effective temperatures.) Figure 10 shows the colors of the Lenz et al. (1998) models, along with the colors of the six stars for which spectra exist, and the colors of the BSs and horizontal branch stars in Pal 5. The positions of the Pal 5 stars plotted in Figure 10 are circled in the Pal 5 color-magnitude diagram in Figure 7. One star which appears to be on the horizontal branch of Pal 5 and also in the A-star box is far enough from the center of the globular cluster that its membership is questionable, so it was not included in Figure 10. The adopted separation between BHBs and high gravity stars (thick line in Figure 10) in $u^*g^*r^*$ colors was based empirically on the spectra and photometry obtained here, guided by Lenz et al. (1998) and Wilhelm et al. (1999). The models are valid for stars with $6500 < T_{\rm eff} < 10000K$. A few candidate RR Lyraes, selected as in Ivezic et al. (2000), are also indicated.

4.3. Subsamples of A-colored stars

Applying the color separation in Figure 10, the 3126 stars in the northern sample are split into 2041 candidate blue straggler stars and 1085 candidate BHB stars. The southern sample split into 674 candidate blue straggler stars and 408 candidate blue horizontal branch stars. The wedge diagrams for these separated stars are shown in Figure 11 (BHBs only) and Figure 12 (BSs only). These plots separate and enhance the contrast of the structures found in Figure 3, supporting the identifications in §4.1. The structures are interpreted as an elongated arc of BHB stars at $g^* \sim 19$ in the North, and an arc of BS stars about 2 magnitudes fainter in the same direction in the North. Additionally, an arc of BS at about $g^* \sim 20$ is apparent in the South. Both the northern and southern structures extend over 30 degrees or more of the sky. The SDSS stripe is 2.5° wide in declination and so these large structures may extend well beyond the narrow stripes observed here.

One also detects the candidate BHB stars associated with the candidate BS stars in the southern structure. Figure 13 shows histograms of the candidate BS and BHB stars in the RA ranges of the northern and southern structures as a function of magnitude. While there are no significant structures apparent at $\alpha < 200°$ in the North (left panels), the plot clearly shows an overdensity of BHB stars at $g^* \sim 19$ in the North at $\alpha > 200°$ (middle panels) and also shows the overdensity in BHBs at $g^* \sim 18$ in the South (right panels).

The BS/BHB color-color separation is far from razor sharp. Figure 11, for example, which should show the absence of the second fainter arc from the candidate BHB star set and leave only the brighter arc in the north, does not do this completely. This is expected, since the color separation technique does not definitively separate the two populations of stars (see Figure 10). The separation is less effective at fainter magnitudes, where the errors are larger, and at redder colors, where the populations overlap in color-color diagrams.

The $g^* - r^*$ color distribution of candidate BS and BHB stars in the large structures in the North and South is histogrammed in Figure 14. In the upper panel, candidate BSs with $\alpha > 200°$

and $g^* > 20$ in the Northern structure are indicated with a light line against $g^* - r^*$ color, while candidate BHBs ($18.8 < g^* < 19.4$) in the same area are histogrammed with a heavy line. The lower panel shows the Southern structure objects with $19.0 < g^* < 20.5$ BSs and $17.7 < g^* < 18.3$ BHBs. In this color system, an A0V main sequence star has $g^* - r^* = -0.25$, whereas a somewhat cooler A5V star will have $g^* - r^* \sim -0.05$. The distribution of BS stars in Figure 14 shows that the BS candidate stars are consistent with intermediate (A3-A5) A star colors, and the population is not dominated by the hottest A0 colored objects. The BS candidate sample is also notably consistent with the Pal 5 BS objects of Figure 7, which also doesn't contain any BS stars as hot as an A0 dwarf.

One might naively expect the A colored stars in the Sextans dwarf irregular galaxy to represent its horizontal branch. However, van Dyk, Puche, & Wong (1998) show that this galaxy has a young very blue main sequence; if there is a horizontal branch, it contains very many fewer stars. The ratio of the number counts of BS:BHB candidates is 36:19 for the Sextans dwarf. This ratio is similar to the ratio of the excess of BS candidates at $g^* \sim 20$ to the excess of BHB candidates in the same magnitude range in the southern structure. In both cases, we assume that the candidate BHBs are misidentified high surface gravity stars. Thus for Sextans, nearly all the BS and BHB candidates are simply young main sequence stars.

4.4. Simulation of a Spheroidal Halo

The tight concentration of BHB magnitudes in Figure 13 and the existence of associated BS candidate stars are strong evidence that the northern and southern structures are real halo substructure. However, one must explore the possibility that these structures could be artifacts of a smoothly varying galactic structure combined with the magnitude limits of the SDSS samples. One is concerned with the possibility that the northern structure might be associated with the bulge of the Milky Way, since it occurs at a Galactic longitude of zero degrees.

Figure 15 shows a simulated halo density distribution expected for a smooth spheroidal distribution of BHB stars, assuming $M_{g^*}(\mathrm{BHB}) = +0.7$, $\alpha = -3.0$, and $c/a = 1.0$. One can see from this figure that the highest density of BHBs is closer to the Galactic plane in the equatorial stripe (indicated by the line of nodes in Figure 15), than to Galactic longitude of zero. This is because the plane of the celestial equator passes closer to the center of the Galaxy at the Galactic plane than at Galactic longitude of zero. The halo density distribution depends only on the distance from the Galactic center for a spherically symmetric halo population.

One must resort to an extremely unlikely model to reproduce an over-density such as that seen in Figure 3 within a smooth spheroid. For example, assuming an unrealistic absolute magnitude of $M_V \sim +4$ for the A-colored stars, and an extremely prolate ($c/a = 3$) bulge, one can obtain an overdensity near $l = 0$, but it will be much more spread out in magnitude than the tight BHB locus seen at $g^* \sim 19$. Additionally, such an exercise can in no way reproduce the observed overdensity

in the South with the same smooth model. The southern structure is nearly directly opposite the Galactic center.

4.5. Distribution of redder Galactic stars

Figure 16 shows a wedge plot, similar to Figure 3, but for F star candidates (objects with $0.6 < u^* - g^* < 1.0$, $0.1 < g^* - r^* < 0.3$), which are intrinsically about 3 magnitudes fainter than BHB stars. One sees here the familiar overdensity in the southern sample, but the typical magnitude, $g^* \sim 21$, is about one magnitude fainter than that of the presumed BSs of Figure 12. This indicates that one may be detecting F stars associated with the southern structure ($g^*_{BHB} = 18$). Note that although the density of the F star concentration appears to fall off near $\alpha = 49°$, the density of QSOs in Figure 4 also drops off in this region at about 21^{st} magnitude in g^*, indicating that the sample is less complete in that region.

The rest of the F star distribution is consistent with a smooth Galactic model. (Imagine shifting the model distribution in Figure 15 three magnitudes fainter.) The halo F stars associated with the northern structure are too faint to be unambiguously detected with the SDSS.

A magnitude-RA wedge plot for color-selected G stars for the same SDSS samples is presented in Figure 17. It is reassuring to see no signs of the northern or the southern structures in this wedge plot; the G stars ($M_V \sim +5$) associated with these structures are too faint to appear above the SDSS magnitude limits. This population may prove valuable for studies of Galactic structure at closer distances than those probed by the BHB/BS stars. A slight leak of F stars in to the G star box may be manifesting itself as structure in the South at $g^* \sim 21.5$.

5. PROPERTIES OF THE LARGEST STRUCTURES

As horizontal branch stars have $M_{g^*} \sim 0.7$ and BS stars have $M_{g^*} \sim 2.7 \pm 1.0$, one can estimate the heliocentric distances to the largest structures using the simple magnitude-distance relation, $\mathrm{m} - \mathrm{M_{g^*}} = 5\log(\mathrm{d_{pc}}) - 5$. Assuming the Sun is 8 kpc from the Galactic center, one can then use [l,b] for each object and calculate a Galactocentric distance for each star. The resulting Galactocentric distance estimates are plotted as (α, $\mathrm{R_{GC}}$) polar wedge diagrams in Figure 18 (for the BHB subsample) and Figure 19 (for the BS subsample). The implied distance of the large clump of stars in the North is 46 kpc from the Galactic center, with Galactic rectangular coordinates extending from (X,Y,Z) = (12, -13, 41) to (26, 1, 34) centered at (X,Y,Z) = (21, -5, 38) [units are kpc, where the sun is at (-8,0,0)]. The most significant clump in the south is inferred to be about 33 kpc from the GC extending from (X,Y,Z) = (-18, 9, -25) to (X,Y,Z) = (-25, 3, -22) centered at (-22, 6, -24). The significance of other smaller clumps seen in Figures 18 and 19 is tantalizing, and merits kinematic followup to determine if they are moving groups or streamers. In this coordinate system, Sextans is at (-36, -53, 58) and Pal 5 is at (7, 0, 16).

Because of the small declination coverage currently available, the full extent of these large halo structures is not known. However, an extent of 30 degrees in RA at 46 kpc, with a 'depth' of at up to ten kpc (from the spread in magnitudes in Figure 13), suggests a structure of extent at least 20 kpc by at least 2 kpc by up to 10 kpc. A significant fraction of the assumed width from the magnitude spread could be due to the intrinsic spread in the absolute magnitudes of BHB stars, and the actual structures could in fact be extremely long and narrow "streams". One can estimate the implied total mass for the large structures in the northern and southern samples from the number of BHB stars observed. From the data associated with Figure 13, one estimates that there are 200 BHB stars (above background) in the northern structure. To arrive at this estimate, one uses the counts per square degree of BS and BHB stars in the left hand panel in Figure 13 to estimate the background; the counts above background are assumed to be associated with the structures. Excess counts at $g^* \sim 19$ in the northern sample and at $g^* \sim 18$ in the southern sample were assumed to be BHB stars. Likewise, excess counts at $g^* \sim 21$ in the northern sample and at $g^* \sim 20$ in the southern sample were assumed to be BSs.

In Pal 5, there are five BHB stars in the sample. From comparisons of the total magnitude of Pal 5 to other globular clusters as tabulated in Djorgovski & Meylan (1993), we estimate the mass of Pal 5 to be $1.5 \times 10^5 M_\odot$. Scaling up from a globular cluster mass, a lower limit on the inferred mass in the part of the northern structure detected is then $6 \times 10^6 M_\odot$. This is roughly consistent with estimates of the mass from extrapolations from the number of RR Lyrae stars. Ivezic et al. (2000) detect nearly 80 RR Lyrae variables at $\sim 50\%$ efficiency within the northern clump, as compared to five in Pal 5, giving a ratio of 160 to five as compared with the above ratio of 200 to five. An estimated 60 BHB stars in the southern structure implies a lower limit for the mass of $2 \times 10^6 M_\odot$. There is of course no way to tell what fraction of the structure is detected; more data from the SDSS survey will eventually be able to map out the full extent of such structures.

It is interesting to calculate the ratio of BS:BHB stars in the large structures. In the globular cluster Pal 5, in the color range $-0.3 < g^* - r^* < 0$, there are 7 BS stars and 5 BHBs for a ratio of 1.4:1. In the northern clump, an estimate of 450 BSs is made by assuming a background similar to that in the upper left hand panel of 13, giving a ratio of 2.2:1 when combined with the 200 BHBs seen. The BSs are near the limit of detection in the north, and the sample is incomplete, so the ratio may be considerably larger. For the southern structure, about 380 BSs are estimated, compared with about 60 BHBs, for a ratio of 6:1, with considerable uncertainty. For A-colored stars in the field not associated with the clumps, a ratio of about 2:1 is estimated by the same technique. Preston, Beers, and Shectman (1994) explore the populations of blue stars located at $d < 2$ kpc and find a relatively large specific ratio of blue metal poor to field horizontal branch objects (which are similar to the BS and BHB categories characterized here, though based on somewhat different selection criteria). This apparent variation in the BS:BHB ratio between globular clusters, in the field and in the northern and southern structures, while still somewhat uncertain, appears to be a significant effect, indicating different populations of stars populate different regions of the halo.

The large angular extent and relatively low surface brightness of these structures leads one

to believe that these may be tidally disrupted streamers in the halo. The fact that two such structures were detected in 370 square degrees of data ($\sim$ 1% of the sky) leads one to ask how common these structures might be in the Galactic halo. If the distribution of these objects is uniform across the sky, there may be as many as 200 of these to 20^{th} magnitude in g^*. Since the size of the structures parallel to the line of sight could be as large as 10 kiloparsecs, the area effectively surveyed may be up to five times larger than the survey area (since the width of the stripe is approximately 2 kpc at 19^{th} magnitude). In this case the total expected number of such structures in the halo would be 40, or fewer if the length of each streamer is much greater than 20 kpc. The existence of such structures lends strength to the argument that some or all of the halo of our Galaxy has been formed through the accretion, or at least the disruption, of smaller stellar systems (Majewski 1994). Numerous studies have found evidence for coherent structures in the halo using kinematic information. Majewski, Munn, & Hawley (1994) found a clump of 6–9 halo stars about 4–5 kpc above the North Galactic Pole with very similar radial velocities and proper motions and identified a moving group. Helmi & White (1999) simulate satellite galaxy disruption and phase-space diffusion in the halo and suggest that the halo could consist of 300–500 streams with components that pass close to the sun, a number consistent with that estimated above. Earlier, Doinidis & Beers (1989) noted a group of 7 field horizontal branch stars with similar radial velocities all within 1 square degree on the sky and furthermore noted a positive signal in the 2-point star-star correlation function of A-colored objects on scales of $10'$.

A cross-check against 21 cm emitting High Velocity Clouds (Wakker & van Woerden 1997) does not show any obvious positional matches with these large structures in the north and south, but if even small amounts of gas is associated with the structures, a scenario such as that described in York et al. (1986) could hold, where the halos of galaxies are full of small complex, quasar absorption line producing structures. If the structures are as numerous as 100 in the halo, then they could contain a few$\times 10^8 M_\odot$, a significant fraction of the luminous halo. This is corroborated by Figure 13, from which one estimates that one in four of the BHB stars in the combined samples are in one of the two large clumps (using the color separation of stellar types for field stars, and magnitude separation of the stellar types in the clumps).

To review: For the structure in the north, one sees BHB and BS candidate stars and for the structure in the south, which is closer, one sees these related populations of stars: BHB candidates, BS candidates, and F stars in numerical proportions which are not completely out of line with expectations from globular clusters or that of known galactic populations. The rough mass estimates for the structures are somewhat above that for a massive globular cluster, and only a factor of a few smaller than that of known dwarf companions to the Milky Way. Thus galaxies like Ursa Minor or the Draco dwarf spheroidal at about 70 kpc from the Galactic center, which currently have central stellar densities much higher than those inferred for the extended structures in the north and the south, could provide progenitors of the low density structures seen in Figure 3. It should be noted that the mass estimates from BHB stars is highly uncertain, and assumes similar horizontal branch structure for all populations. If BS counts were used, the mass estimates would be several times

higher.

6. FITS TO THE GALACTIC HALO MODEL

The discovery of extensive structures in the outer Galactic halo is extremely interesting, and the number of A-colored stars associated with structures is of the same order as that in a supposed smooth background distribution of halo tracers. This renders attempts to fit a smooth spheroid model with a single values of α and c/a problematic. The approximate separation of BHB and BS stars in §4.3, however, can be used to try and isolate only BHB tracers, and if one restricts that sample further to avoid the obvious clumps, one may still attempt a significant fit to a smooth spheroid. Figures 20 shows a maximum likelihood fit to flattened spheroidal models of BHB candidate stars in the North and South. Fits were restricted to those BHB color candidates with implied R < 40 kpc, to regions which avoided the clump at $g^*(BHB) = 18$ in the south, and to regions which avoided saturated detections of stars (which occurs in the SDSS at about $g^* \sim 15$, $d \sim 7$ kpc). Constraining the fit to match the numbers of objects seen in the North and South simultaneously helps greatly in restricting parameter space. The model fit uses $\rho \sim R^{\alpha}$, where $R^2 = (X^2/a^2 + Y^2/b^2 + Z^2/c^2)$, and X, Y, Z are Galactic rectangular coordinates. Setting $a = b = 1$, α and c are allowed to vary.

The maximum likelihood estimate of the halo structure parameters for $7 <$ d < 40 kpc is: $\alpha = -3.2 \pm 0.3$, $c/a = 0.65 \pm 0.2$, in agreement with Gould, Flynn, & Bahcall (1998) and many other authors. Models with $c/a = 1.0$ or $\alpha < -2.8$ yield significantly worse fits to the sample. After the numerous cuts placed on the input candidate sample, the number of stars fit is 527 stars. The fit can be extrapolated to provide a local density for BHB stars at a distance of 8 kpc from the Galactic center. This normalization yields $\rho_{\rm BHB}(8\,{\rm kpc}) = 8\,{\rm kpc}^{-3}$, in reasonable agreement with earlier studies (Kinman, Suntzeff & Kraft 1994).

More data, and cleaner spectroscopic separation of BHB from BS stars will of course help improve the confidence in these numbers to $r > 40$ kpc, though if the presence of enormous structures in the outer halo at larger radii is pervasive, fitting a single set of parameters to the shape of the outer halo may not provide much insight into its overall mass distribution.

7. CONCLUSIONS

1. A sample of 4208 A-colored stars from the SDSS is uniform to $g^* = 19.5$ and extends to $g^* \sim 22$. This sample is used to probe halo structure at distances of up to 60 kpc from the Galactic center.

2. A plot of all A-colored stars in magnitude-angle space shows significant clumpiness, including a large structure in the North at (α, δ) = (220°, 0°) extending over 30 degrees in length and at least 2.5 degrees in width. The remarkable detection of a clump of 80 RR Lyraes in

this same area of sky by Ivezic et al. (2000) demonstrates the coherence and existence of this structure. In the South, a second extended structure of over 20 degrees in length is apparent. Numerous smaller structures, including the known dwarf irregular Sextans (at 75 kpc from the Galactic center) and the Globular cluster Pal 5 are also clearly visible.

3. The example of Pal 5, which has a BHB and a BS sequence two magnitudes below its BHB, suggests an explanation for the parallel magnitude-angle-space arcs seen in the larger blue star halo samples. Photometric separation of A star surface gravities supports this explanation. A majority of the high surface gravity A-colored stars in the halo may be BSs.

4. Based on followup spectroscopy of eight objects, there are at least two sub-populations of A-colored stars identified: blue horizontal branch stars with low surface gravities, and blue straggler stars with high surface gravities and absolute magnitudes one to three magnitudes fainter than the horizontal branch.

5. The assumption of $M_{g*} \sim 0.7$ for the horizontal branch yields approximate distances to the large clumps in the North and South of 46 kpc and 33 kpc from the Galactic center at positions (X,Y,Z) = (21, -5, 38) and (-22, 6, -24) kpc, respectively. The inferred masses of the detected structures is at least $6 \times 10^6 M_\odot$ in the north and at least $2 \times 10^6 M_\odot$ in the south, though it is not known what fraction of the total extent of these elongated structures has so far been detected. From estimates of the mass in these structures and the fraction of sample BHB stars they contain, one concludes that structures such as these could contain a significant fraction of the mass of the luminous halo.

6. Fitting the 'field' BHB candidate stars, (those which avoid the structures), while requiring a consistent normalization between northern and southern Galactic samples, yields a maximum likelihood fit to a spheroidal halo model of $\alpha = -3.2 \pm 0.3$ and flattening of $c/a = 0.65 \pm 0.2$ for $7 < R < 40$ kpc, consistent with previous work. Since clumps of A-colored objects dominate the numbers of halo BHBs and BSs at distances > 30 kpc, however, simple parameter fits to single spheroid models are not representative of the whole picture. The existence of enormous structures in the outer halo must be addressed.

We acknowledge useful discussions with R. Kron, B. Gibson and many important suggestions and comments from the referee, T. Beers. We thank R. McMillan and K. Gloria for excellent assistance in operating the APO 3.5m telescope.

This work was supported by Fermi National Accelerator Laboratory, under U.S. Government Contract No. DE-AC02-76CH03000.

SALM acknowledges partial support from the Department of Energy at the Lawrence Livermore National Laboratory under contract W-7405-ENG-48 and from the NSF (grant AST-98-02791).

The Sloan Digital Sky Survey (SDSS) is a joint project of The University of Chicago, Fermilab, the Institute for Advanced Study, the Japan Participation Group, The Johns Hopkins University, the Max-Planck-Institute for Astronomy, Princeton University, the United States Naval Observatory, and the University of Washington. Apache Point Observatory, site of the SDSS, is operated by the Astrophysical Research Consortium. Funding for the project has been provided by the Alfred P. Sloan Foundation, the SDSS member institutions, the National Aeronautics and Space Administration, the National Science Foundation, the U.S. Department of Energy, and Monbusho. The SDSS Web site is http://www.sdss.org/.

REFERENCES

Beers, R. C., Preston, G. W., Shectman, S. A., Doinidis, S. P., and Griffin, K. E. 1992, AJ, 103, 167

Chiba, M., and Beers, T. C. 2000, AJ, in press, astro-ph 0003087

Djorgovski, S. G., & Meylan, G. in "Structure and Dynamics of Globular Clusters", eds. Djorgovski, S. G., & Meylan, G. 1993, ASP Conf Series 50, 370.

Doinidis & Beers 1989, ApJ, 340, L57

Eggen, O. J., Lynden-Bell, D., and Sandage, A. 1962, ApJ, 136, 748

Fan, X., et. atl. 2000, AJ, 119, 1

Fukugita, M., Ichikawa,T., Gunn, J. E., Doi, M., Shimasaku, K., Schneider, D. P. 1996, AJ, 111, 1758

Gliese, W. & Jahreiss, H. 1979, A&AS, 38, 423

Gould A., Flynn, C. & Bahcall, J. N., 1998, ApJ, 503, 798

Gunn, J. E. et al. 1998, AJ, 116, 3040

Harris, W. E. 1976, AJ, 81, 1095

Helmi, A., & White, S. D. M. 1999, MNRAS307, 495

Helmi, A., White, S. D. M., de Zeeuw, P. T., and Zhao, H., 1999, Nature, 402, 53

Houk, N., & Smith-Moore,M. 1988 "Michigan catalogue of Two-Dimensional spectral types for the HD stars, vol. 4" Univ of Michigan.

Ibata, R. A., Gilmore, G., and Irwin, M. J. 1995, MNRAS, 277, 781

Ivezic et al. 2000, AJ, submitted.

Johnston, K. V. 1998, ApJ, 495, 297

Johnston, K. V., Majewski, S. R., Siegel, M. H., Reid, I. N., & Kunkel, W. E. 1999, AJ, 118, 1719

Kinman, T. D., Suntzeff, N. B. & Kraft, R. P. 1994, AJ 108, 1722

Kurucz, R. L., in Precision Photometry: Astrophysics of the Galaxy, ed. A. G. D Philip, A. R. Upgren, & K. A. Janes 1991 (Schenectady:Davis), 27

Layden, A., Hanson, R., Hawley, S. L., Klemola, A. R., and Hanley, C. J. 1996, AJ, 112, 2110

Lenz, D. D., Newberg, H. J., Rosner, R., Richards, G. T., and Stoughton, C. 1998, ApJS, 119, 121

Lupton, R. H., Gunn, J. E., & Szalay, A. S. 1999, AJ, 118, 1406

Lynden-Bell, D., & Lynden-Bell, R. M. 1995, MNRAS, 275, 429

Majewski, S. R. 1994, ApJ, 431, L17

Majewski, S. R. 1999, In The Third Stromlo Symposium: The Galactic Halo, eds. B. K., Gibson,T. S. Axelrod, and M. E. Putman, ASP Conf. Ser., 165, 76

Majewski, S. R., Munn, J. A., & Hawley, S. 1994, ApJ, 427, L37

Newberg, H. J., Richards, G. T.,Richmond, M., and Fan, X. 1999, ApJS, 123, 377

Norris, J. E., and Hawkins, M. R. S.1991, ApJ, 380, 104

Pier, J. R. 1983, ApJS, 53, 791

Preston, G. W., Beers, T. C., & Shectman, S. A. 1994, ApJ, 108, 538

Preston, G. W., Shectman, S. A., & Beers, T. C. 1991, ApJ, 375, 121

Rodgers, A. W., and Roberts, W. H. 1993, AJ, 106, 2294

Rodgers, A. W., Harding, P., and Sadler, E. 1981, ApJ, 244, 912

Saha, A. 1985, ApJ, 289, 310

Schlegel, D. J., Finkbeiner, D. P., Davis, M. 1998, ApJ, 500, 525

Sills, A., and Bailyn, C. D. 1999, ApJ, 513, 428

Sluis, A., & Arnold, R. 1998 MNRAS, 297, 732

Sommer-Larsen, J., Christensen, P. R., and Carter, D. 1989, MNRAS, 238, 225

Stryker, L. L. 1993, PASP, 105, 1081

van Dyk, S. D., Puche, D., & Wong, T. 1998, AJ 116, 2341

Wakker, B. P. & van Woerden, H. 1997, ARA&A 35, 217

Wetterer, C. J. & MacGraw, J. T. 1996, AJ 112, 1046

Wilhelm, R., Beers, T. C., Sommer-Larsen, J., Pier, J. R., Layden, A., C., Flynn, C., Rossi, S., Christensen, P. R. 1999, AJ, 117, 2329

York, D. G., Dopita, M., Green, R., Bechtold, J. 1986 ApJ 311, 610

York, D.G. et al. 2000, AJ, submitted.

Zinn, R., 1985 ApJ 293, 424

Fig. 1.— $u^* - g^*$ vs. $g^* - r^*$ color-color diagram for SDSS commissioning data on the celestial equator. The plot shows the colors of $\sim 30,000$ stars from 13.3 square degrees of commissioning data in the range $165° < \alpha < 225°$, $-0.23° < \delta < 0.0°$. This represents 4 hours of observations from one of six columns of CCDs in the imaging camera. Each column of CCDs images a strip of sky 0.23 degrees wide in five passbands. Objects in different magnitude ranges are shaded differently. The A-colored star selection box is identified, as are boxes for quasar candidates, F, and G type colored stars.

Fig. 2.— The upper line indicates fraction of stars matched between runs 745 and 756 without any restrictions on color. This indicates a detection limit of about $g^* \sim 22.5$ (50%). The lower line shows the fraction of stars in the A star color-color box ($0.8 < u^* - g^* < 1.5, -0.3 < g^* - r^* < 0.0$) that are matched as a function of g^* magnitude. This indicates a uniform completeness limit of about $g^* \sim 20$ in the northern sample. The low matched fraction (80%) at bright magnitudes is due to color errors at the red end of the box ejecting one or another detection of a star from the matched pair out of the color box.

Fig. 3.— A polar wedge plot of RA vs. g^* magnitude for A-colored stars. Notice the parallel arcs at $195° < \alpha < 230°$ and the large structure at $20° < \alpha < 40°$, as well as the Sextans dwarf irregular galaxy at $\alpha = 153°$, $g^* = 20.5$ and the Pal 5 BHB at $\alpha = 229°$, $g^* = 17.3$. The Pal 5 blue straggler sequence is visible as a thin line at $\alpha = 229°$, $18.5 < g^* < 20.5$. The intersection between the plane of the celestial equator and the plane of the Galaxy is indicated by a dark line. Galactic and celestial coordinates are indicated around the edge of the figure. g^* magnitude increases outward from the center. Pal 5 is notable in the enlarged in the small diagram to the right, rotated 90° counterclockwise from the main figure.

Fig. 4.— Wedge plot of RA vs. g^* magnitude for color-selected quasar candidates (objects in the small quasar box of Figure 1 with $-0.05 < u^* - g^* < 0.15, -0.1 < g^* - r^* < 0.0$). This population of almost exclusively extragalactic objects is very uniformly distributed in RA to at least $g^* = 22$ (where there is contamination from F stars with large color errors). This demonstrates the uniformity of the SDSS data sample. The Northern sample reaches about 0.5 mag deeper than the Southern sample due to increased u^* errors for the somewhat lower quality Southern sample data leading to a brighter $u^*_{\rm err} < 0.30$ cutoff in the South.

Fig. 5.— Number counts of quasars in the North and South samples. Densities of extragalactic candidate objects in the large quasar candidate color-color box of Figure 1 ($-0.05 < u^* - g^* < 0.35, -0.1 < g^* - r^* < 0.3$) in the North and South are overplotted. The close agreement between the two curves demonstrates the consistency of the SDSS photometric calibration for this isotropically distributed sample of objects. The magnitude limit in the North is about 0.5 m fainter than that in the Southern sample. The Northern sample reaches about 0.5 mag deeper than the Southern sample due to increased u^* errors for the somewhat lower quality Southern sample data leading to a brighter $u^*_{\rm err} < 0.30$ cutoff in the South.

Fig. 6.— Wedge plot of RA vs. g^* magnitude for A-colored stars selected in independent SDSS runs. Similar to Figure 3, the reality of clumped structures is independently verified. This data set doesn't cross the longitude of Sextans, and since it is only data for one-half of a filled stripe, it only has half the stellar density of the Figure 3. However, the coverage makes the end of the northern structure is more apparent than in Figure 3.

Fig. 7.— Color-magnitude diagram around the globular cluster Pal 5. The blue A-colored object box limits in $g^* - r^*$ are indicated by two vertical lines. Note the 5 BHB stars and 7 candidate blue straggler stars, separated by about 2 magnitudes in g^*. The circled objects indicate the BHB and BS objects. Objects with squared circles were followed-up spectroscopically.

Fig. 8.— Spectra of a Pal 5 BHB and Pal 5 BS star. The upper panel shows the Balmer lines for a horizontal branch star in the cluster Pal 5. The width of the $H\delta$ and $H\gamma$ lines are clearly better matched to the reference BHB star (a $V = 12$ field BHB) than to the reference field A0V star. The horizontal line marks 80% of the continuum of the stars, facilitating the quantitative width measurement. The lower panel shows a Pal 5 blue straggler spectrum, which clearly fits the high gravity reference A0V star.

Fig. 9.— Six ARC 3.5m spectra of SDSS A-colored stars. The star in the lower left is best fit by a high gravity model while the other 5 are narrower and consistent with BHB gravities. The star in the upper left has a narrower line width, and the fluctuating continuum suggests a metal-line enhanced Am star classification.

Fig. 10.— $u^* - g^*$ vs. $g^* - r^*$ color-color plot for stellar models and stars with measured surface gravities. Models from Lenz et al (1998), valid for stars with $6500 < T_{\rm eff} < 10000K$, are plotted in small filled circles (low gravity BHB models) and small open circles (high gravity BS/A models). The range of colors for each model represents a range of metalicities. The eight stars for which spectra were obtained plus other Pal 5 BHBs and BSs are plotted on the diagram as triangles and squares. The heavy black line then represents an empirical separation curve between stars of high and low gravity, and is used to separate the SDSS A-colored star sample into BS candidates and BHB candidates based on colors alone. A few (low-gravity) variable RR Lyraes from Ivezic et al. (2000), put on the color system of this paper, are also indicated.

Fig. 11.— Wedge plot of RA vs. g^* magnitude for stars with colors of candidate BHBs. The well defined horizontal branches of the arcs at $g^* = 19$ in the North and $g^* = 18$ in the south, as well as Pal 5's BHB, clearly stand out in this selection of photometrically selected BHB candidates.

Fig. 12.— Wedge plot of RA vs. g^* magnitude for stars with colors of BSs. The distant (fainter) clumps are defined in intrinsically fainter BS candidate A-colored stars, photometrically separated from the BHBs.

Fig. 13.— Magnitude histograms for candidate BHB and BS stars in the northern and southern structures. The northern diagrams include all blue stars with RA $< 200°$ (left panels), and RA $>$

200° (middle panels), and the southern diagrams include all stars with RA > 0°. There are clearly clustered horizontal branch objects at $g^* = 19$ in the North at $RA > 200°$, and at $g^* = 18$ in the South.

Fig. 14.— $g^* - r^*$ color histogram of all objects in the northern structure (upper panel) with BHB candidate colors and $18.8 < g^* < 19.4$ (thick line) and BS candidate colors and $g^* > 20$ (thin line). The southern structure histograms (lower panel) are objects in the clump with $17.7 < g^* < 18.3$ for BHB candidates (thick line) and $19 < g^* < 20.5$ for BS candidates (thin line). Note that most of the BS candidates are on the red side of the diagram.

Fig. 15.— Wedge plot of RA vs. g^* for a simulated smooth galaxy halo of $M_{g*} = 0.7$ BHBs with $\alpha = -3$ and $c/a = 1$. The entire celestial circle is shown (not just for regions where SDSS data exists). The maximal density of stars is nearly, but not exactly, at $b = 0$. Such a density maximum is a poor fit to the clump seen in Figure 3 (with maximum density at $l \sim 0$, and no equivalent maximum is seen in the south at $l = 180$. This is further evidence that the structures seen in Figure 3 are real halo substructures.

Fig. 16.— Wedge plot of RA vs. g^* magnitude for F star candidates (objects in the box $0.6 < u^* - g^* < 1.0, 0.1 < g^* - r^* < 0.3$. Because of the high relative density of these objects a randomly selected subsample of 1 in 10 points is actually plotted. The F stars in the South at $20° < \alpha < 40°$ at $g^* = 21.5$ are apparently associated with the A-colored star clump. In the North, the Galactic halo distribution overwhelms any clumps. Clump-associated F stars in the North would have magnitudes $g^* \sim 22 - 23$.

Fig. 17.— Wedge plot of RA vs. g^* magnitude for G star candidates ($0.9 < u^* - g^* < 1.3$, $0.3 < g^* - r^* < 0.4$). Because of the relative density of these objects, a randomly selected subsample of 1 in 5 points is actually plotted. The structure of the disk is becoming manifest as one move to lower Galactic latitudes. No trace of the clumps visible in A-colored objects remains for G stars of similar magnitudes. Clump-associated G stars would be at $g^* > 24$. A few F stars may be leaking into the G star box, as indicated by the presence of excess stars near $g^* = 21.5$ in the south.

Fig. 18.— Wedge plot of RA vs. inferred Galactocentric radius for candidate BHB stars. An average absolute magnitude of $M_g = +0.7$ is assumed to infer distances to the BHB photometrically selected sample. Horizontal branch concentrations are visible at R = 46 kpc in the North and R = 33 kpc in the South. Sextans is visible at about 80 kpc. Other structures, such as the one at $\alpha = 194°$, R=50 kpc remain to be confirmed. The limiting magnitude ($g^* \sim 22.5$) allows detection of BHBs out to 150 kpc, but the sample at the faintest limits is contaminated by intrinsically fainter BSs, and so the objects apparently out at $R > 75$ kpc are not confirmed to actually be at these great distances.

Fig. 19.— Wedge plot of RA vs. inferred Galactocentric radius for candidate BS stars. An average absolute magnitude of $M_g = +2.7$ is assumed to infer distance to the BSs. Loose concentrations at R = 46 kpc in the North and R = 30 kpc in the South are visible. The limiting magnitude cuts

off the distribution at about 60–70 kpc.

Fig. 20.— Binned representations of the data and best fit solutions for a simultaneous two parameter fit (plus normalization to the total number of stars) to the stars in the northern and southern BHB candidate (color selected) subsamples after the stars in the large structures have been removed. The panel on the upper left shows the northern sample star counts vs. distance from the sun and a binned likelihood fit model. The upper right panel shows the fit and star count histograms vs. RA. The error bars on the fit represent Poisson statistics for the number of expected objects in the fitted bin. For display purposes, the bin size is 2 kpc in d and 5 degrees in RA. The southern subsample and fits are shown in the lower two panels. The maximum likelihood fit yields $\alpha = -3.2 \pm 0.3$ and $c/a = 0.65 \pm 0.2$.

Table 1 – Spectroscopically targeted A-colored stars

ID	g^*	$u^* - g^*$	$g^* - r^*$	$H_\delta(0.8)$[Å]	l (deg)	b (deg)	Class
CS29516−0011[a]	12.24[b]	1.30[b]	-0.17[b]	21	71	-42	BHB
HD13433	8.16[b]	1.10[b]	-0.14[b]	35	184	-68	A0V
WD0148p467[c]	12.44[b]	0.20[b]	-0.17[b]	60	134	-15	DA WD
SDSSp J151610.80−000745.0	17.20	1.13	-0.20	25	1	46	BHB[d]
SDSSp J151608.00−000821.0	18.88	1.12	-0.13	36	1	46	BS[d]
SDSSp J154256.50−005609.0	17.55	0.99	-0.29	31	6	40	BHB
SDSSp J162341.10+000926.0	17.52	1.18	-0.24	26	14	32	BHB
SDSSp J160326.10+005104.0	17.49	1.18	-0.12	27	11	37	Am
SDSSp J162520.10+000223.0	17.49	0.96	-0.26	33	15	32	A/BS
SDSSp J162025.50−004537.0	17.82	1.11	-0.23	26	13	33	BHB
SDSSp J162532.10−011215.0	17.54	1.11	-0.20	26	13	31	BHB

[a] Ref. Wilhelm et al. 1999

[b] Magnitudes and colors converted from measured U, B, V values

[c] Ref. Gliese & Jahreiss 1979

[d] These objects are in the Globular cluster Pal 5

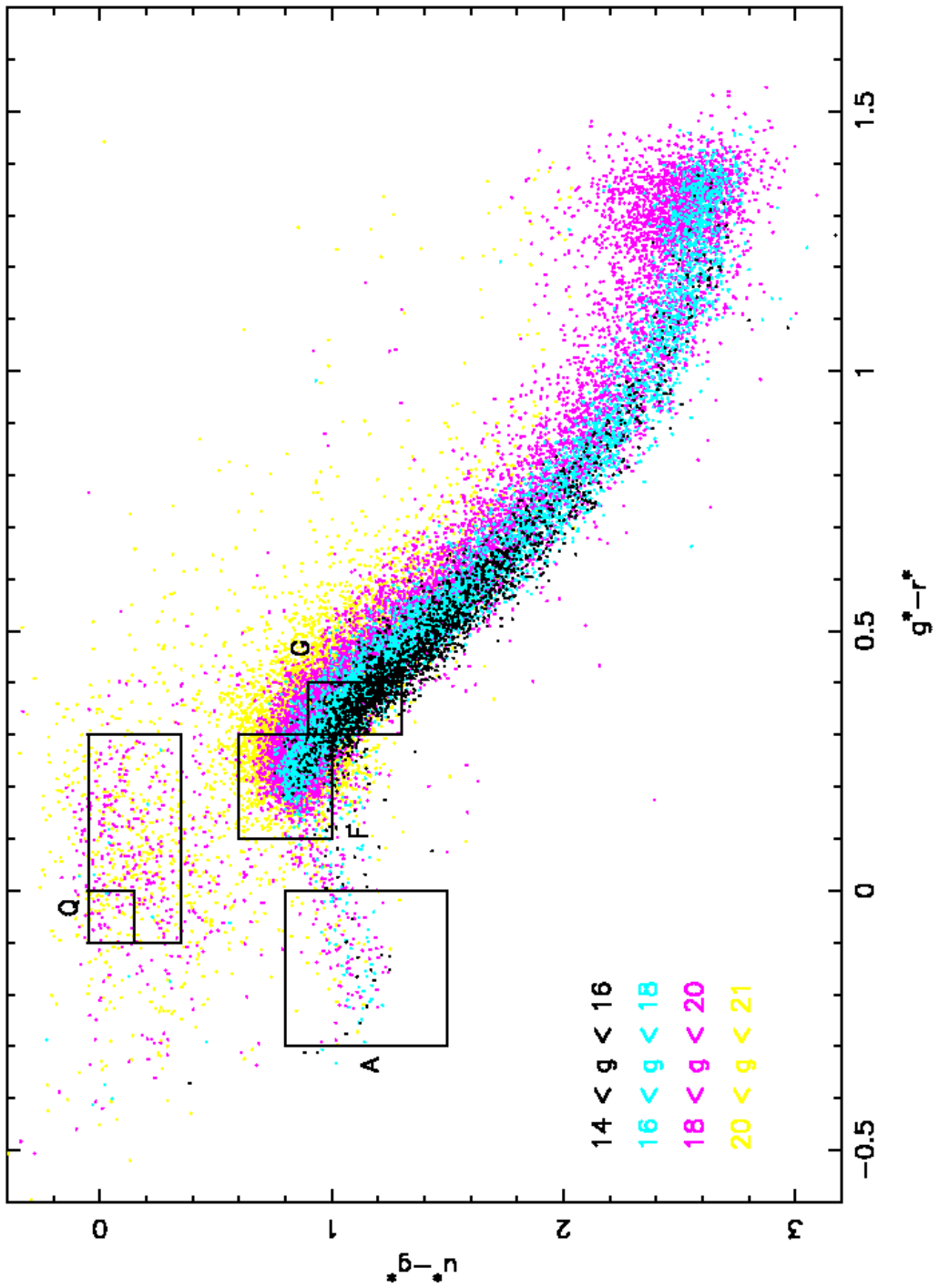
Q
G
F
A
14 < g < 16
16 < g < 18
18 < g < 20
20 < g < 21
u*−g*
g*−r*
0
1
2
3
−0.5
0
0.5
1
1.5

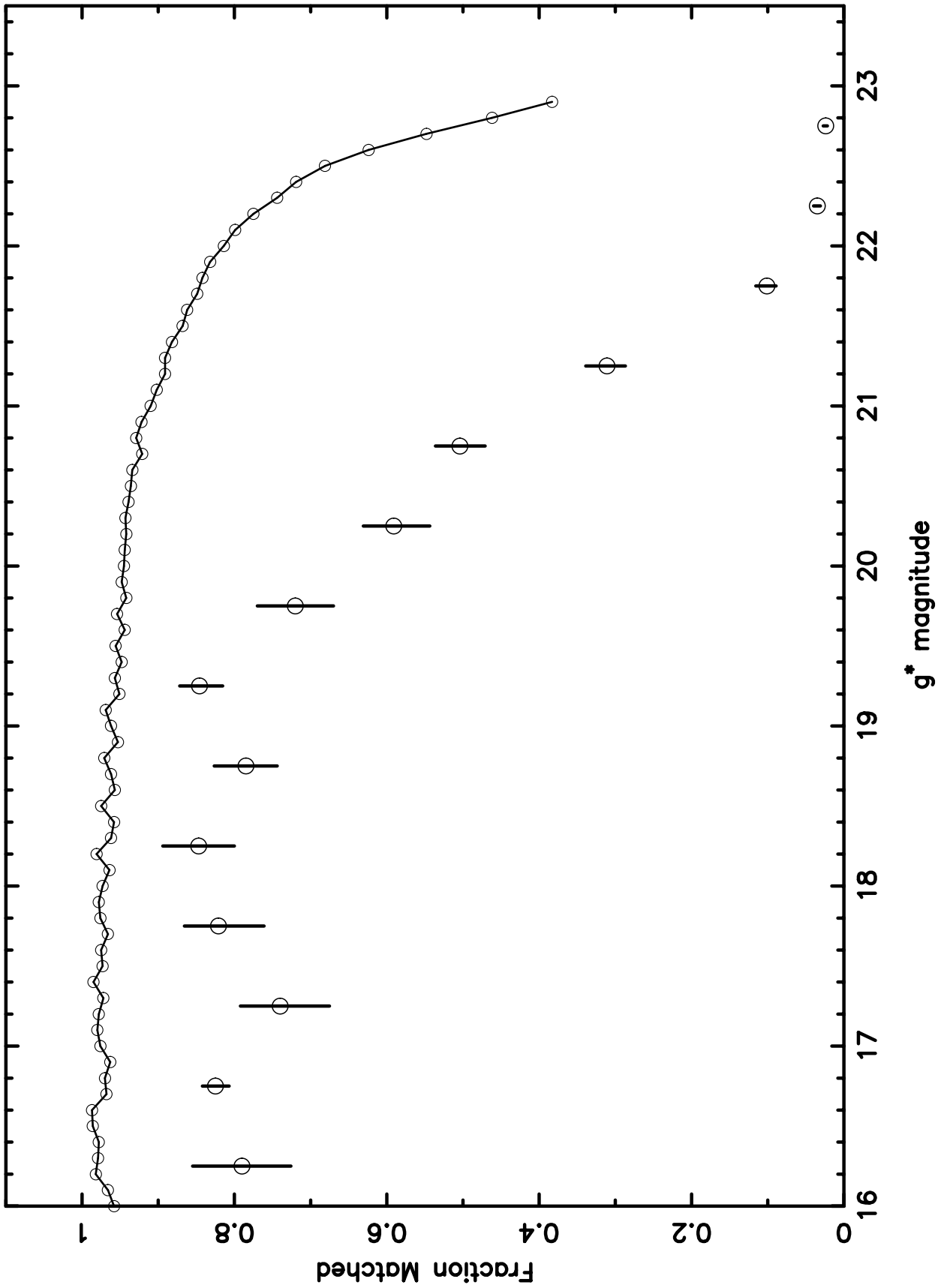
Fraction Matched
0
0.2
0.4
0.6
0.8
1
16
17
18
19
20
21
22
23
g* magnitude

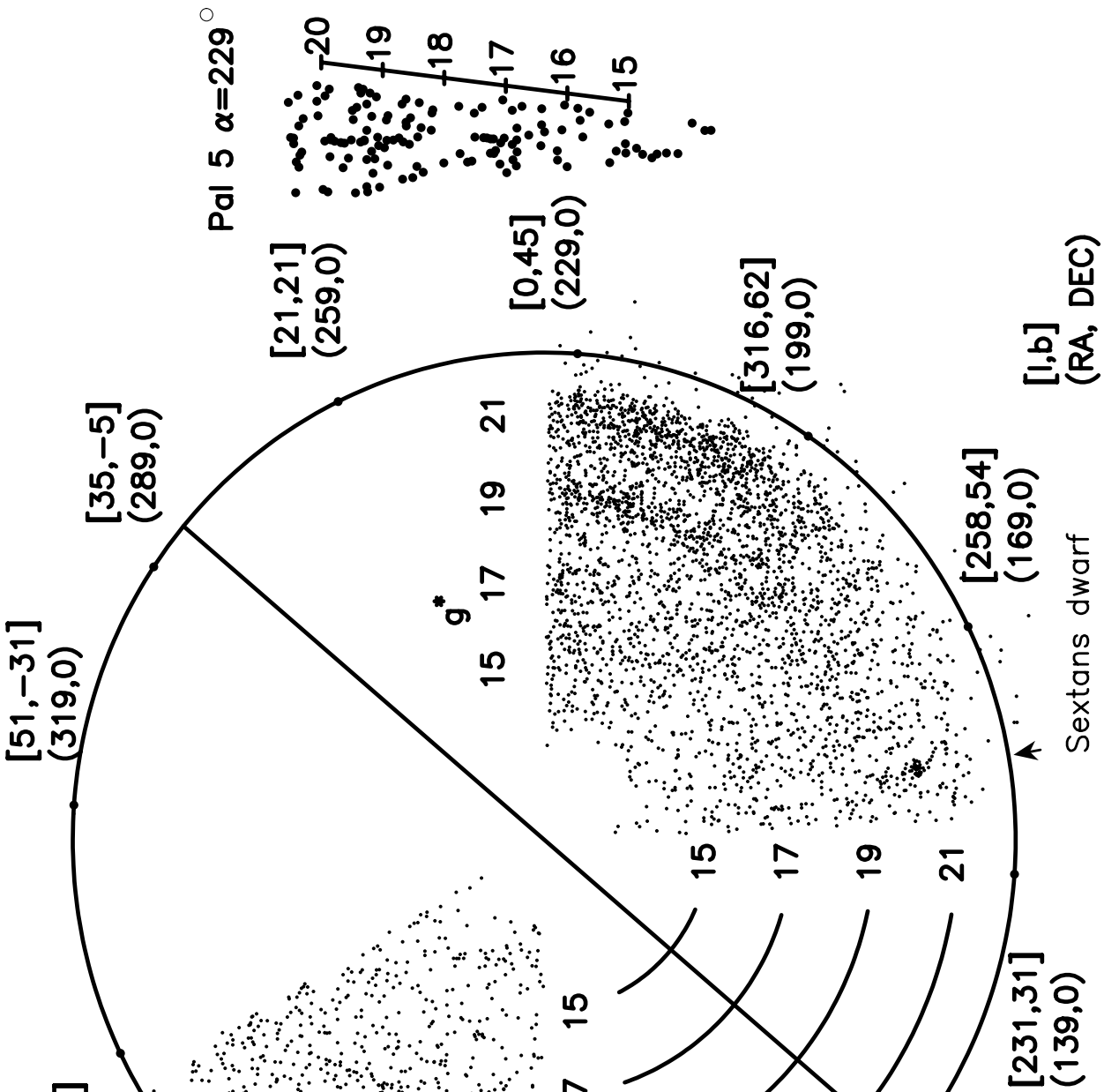
Pal 5 α=229°
20
19
18
17
16
15
[21,21]
(259,0)
[0,45]
(229,0)
[316,62]
(199,0)
[258,54]
(169,0)
[231,31]
(139,0)
[215,5]
(109,0)
[201,−21]
(79,0)
[180,−45]
(49,0)
[136,−62]
(19,0)
[78,−54]
(349,0)
[51,−31]
(319,0)
[35,−5]
(289,0)
g*
15
17
19
21
Sextans dwarf
[l,b]
(RA, DEC)

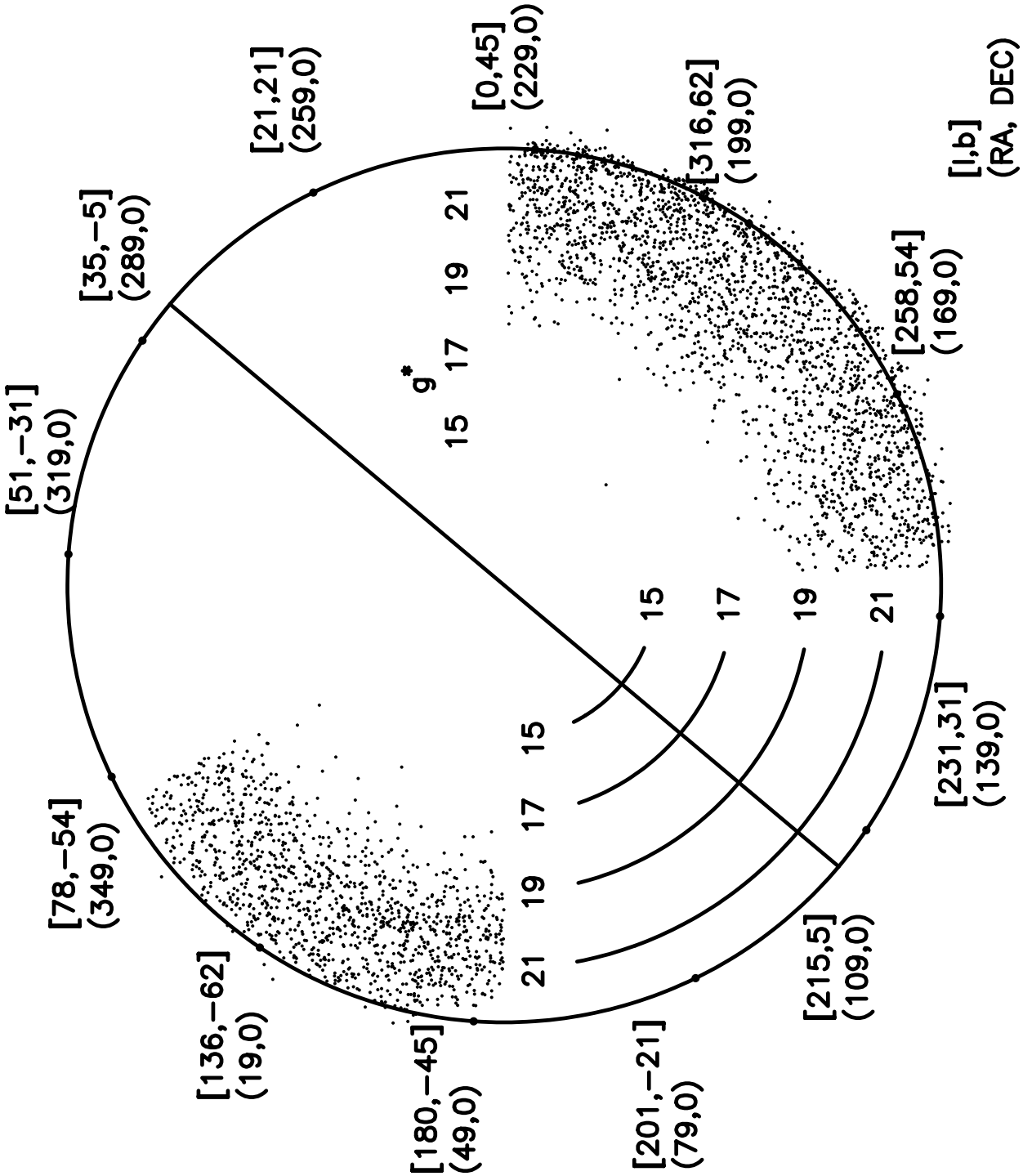
[51,−31]
(319,0)
[35,−5]
(289,0)
[21,21]
(259,0)
[0,45]
(229,0)
[316,62]
(199,0)
[258,54]
(169,0)
[231,31]
(139,0)
[215,5]
(109,0)
[201,−21]
(79,0)
[180,−45]
(49,0)
[136,−62]
(19,0)
[78,−54]
(349,0)
g*
15
17
19
21
[l,b]
(RA, DEC)

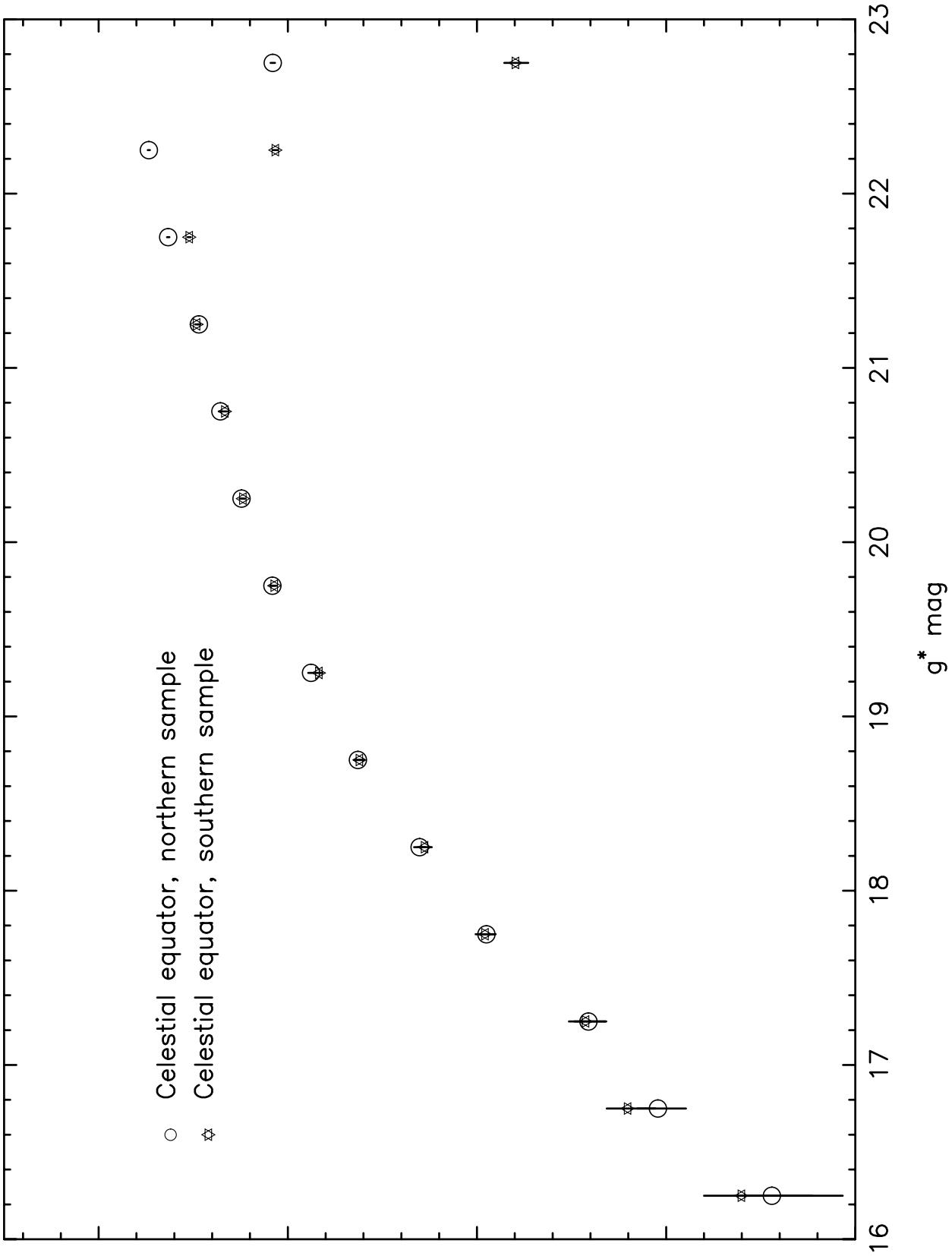
Celestial equator, northern sample
Celestial equator, southern sample
Log10(QSO cand. degree^-2 mag^-1)
g* mag
16
17
18
19
20
21
22
23
-2
-1
0
1
2

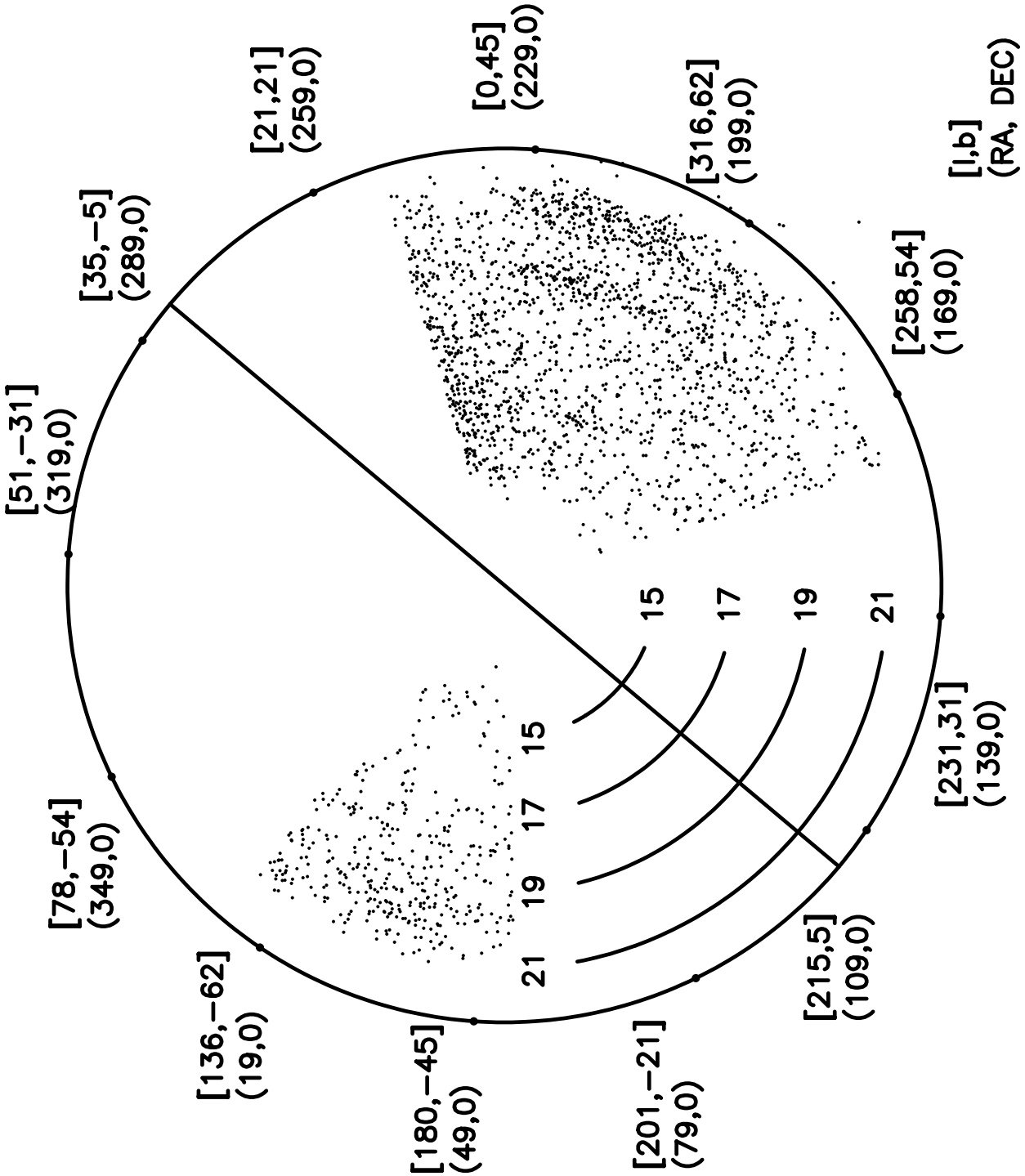
[0,45]
(229,0)
[21,21]
(259,0)
[35,−5]
(289,0)
[51,−31]
(319,0)
[78,−54]
(349,0)
[136,−62]
(19,0)
[180,−45]
(49,0)
[201,−21]
(79,0)
[215,5]
(109,0)
[231,31]
(139,0)
[258,54]
(169,0)
[316,62]
(199,0)
[l,b]
(RA, DEC)
15
17
19
21
15
17
19
21

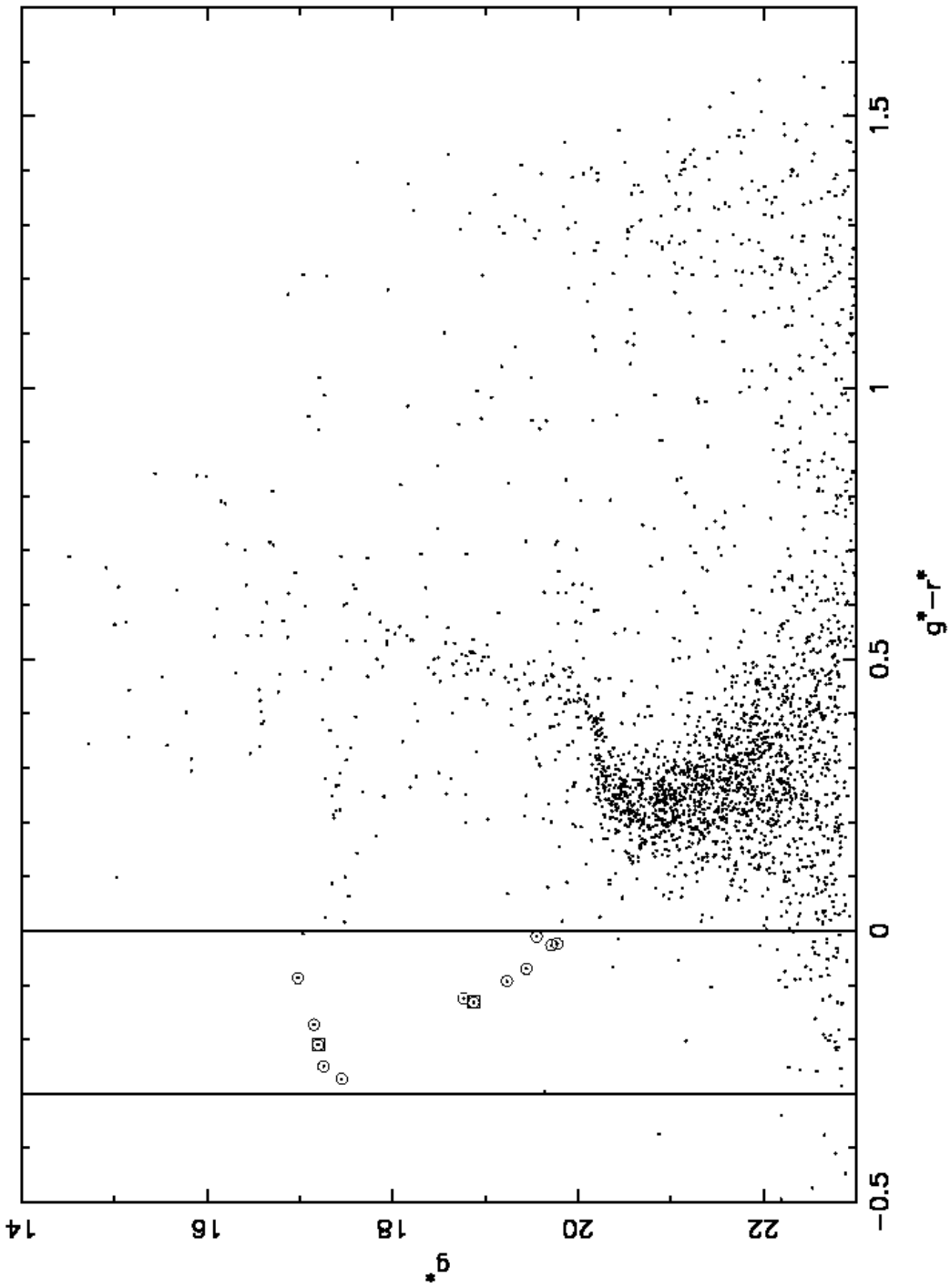
14
16
18
20
22
g*
−0.5
0
0.5
1
1.5
g*−r*

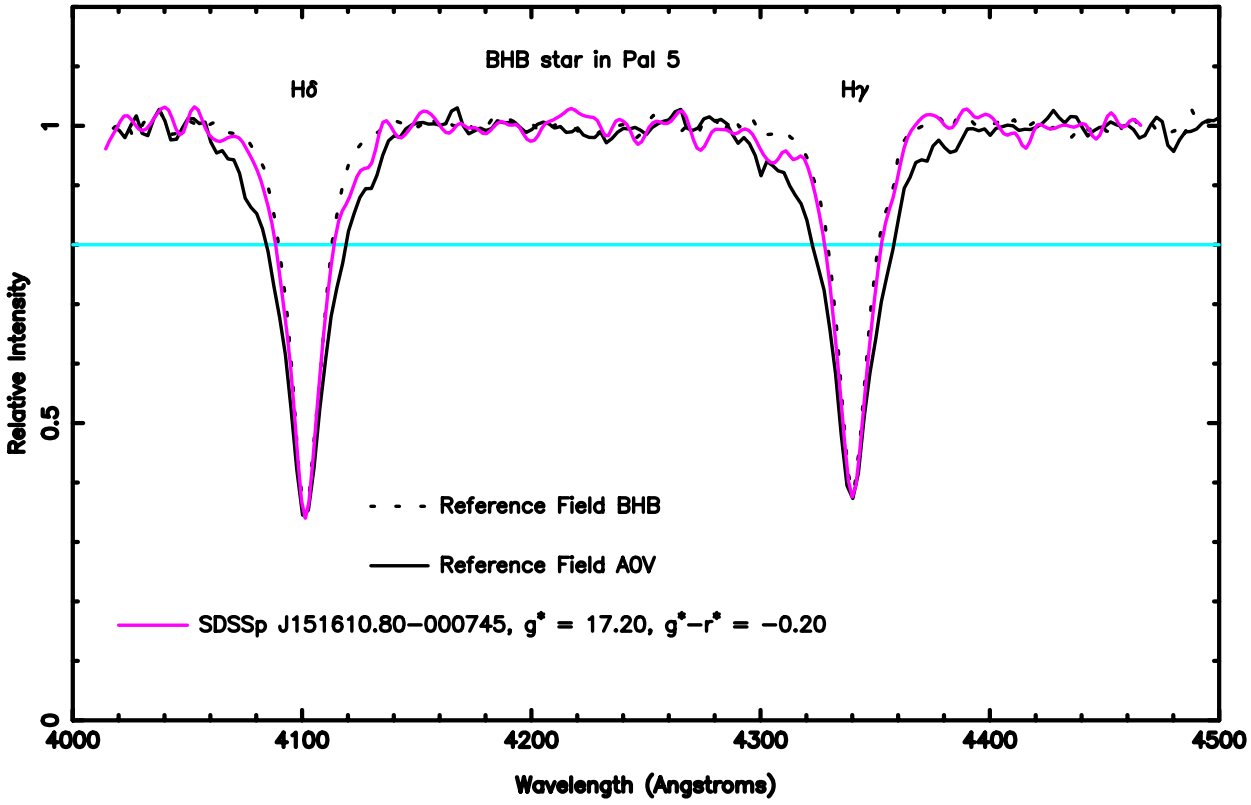
BHB star in Pal 5
Hδ
Hγ
Relative Intensity
0
0.5
1
4000
4100
4200
4300
4400
4500
Wavelength (Angstroms)
- - - Reference Field BHB
Reference Field A0V
SDSSp J151610.80−000745, g* = 17.20, g*−r* = −0.20

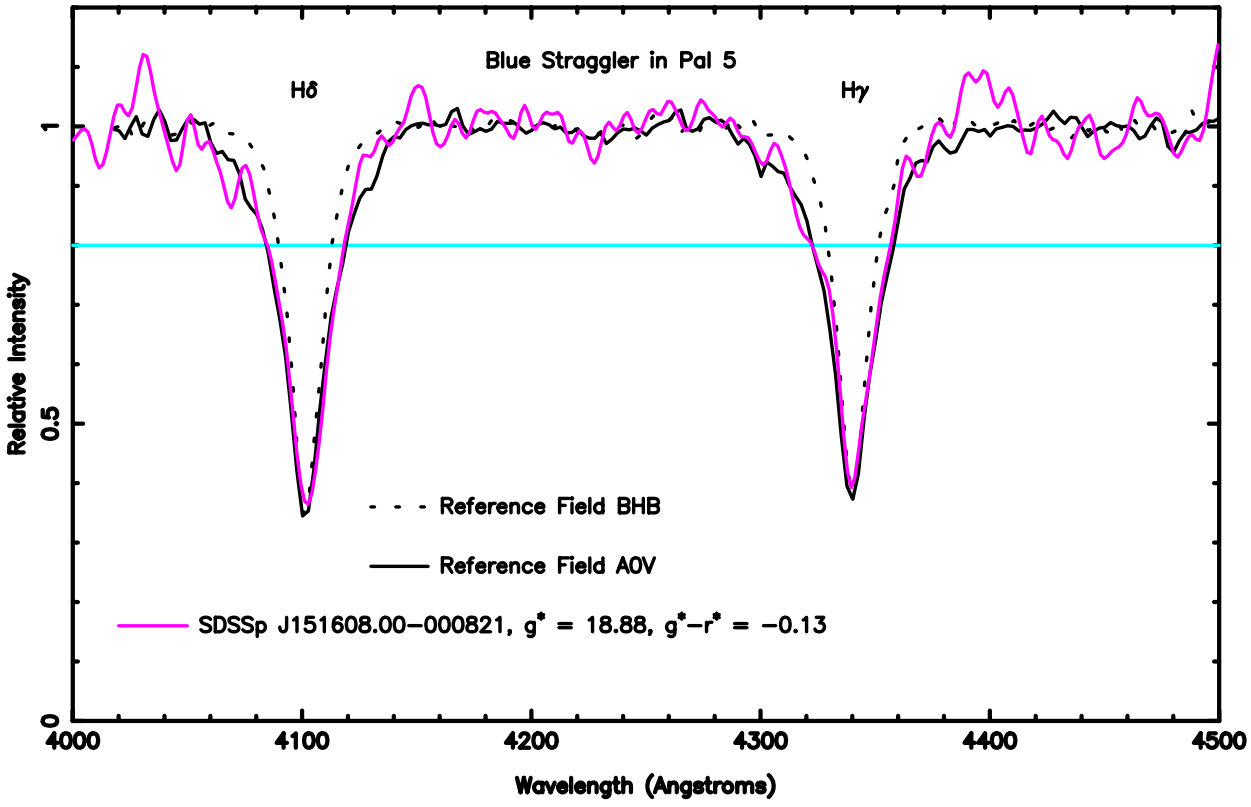
Blue Straggler in Pal 5
Hδ
Hγ
Relative Intensity
0
0.5
1
4000
4100
4200
4300
4400
4500
Wavelength (Angstroms)
- - - Reference Field BHB
Reference Field A0V
SDSSp J151608.00−000821, g* = 18.88, g*−r* = −0.13

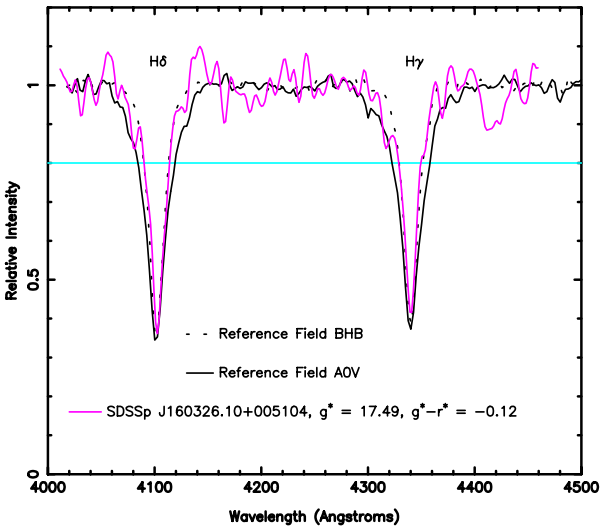
Hδ
Hγ
Relative Intensity
Wavelength (Angstroms)
- - Reference Field BHB
Reference Field A0V
SDSSp J160326.10+005104, g* = 17.49, g*–r* = –0.12

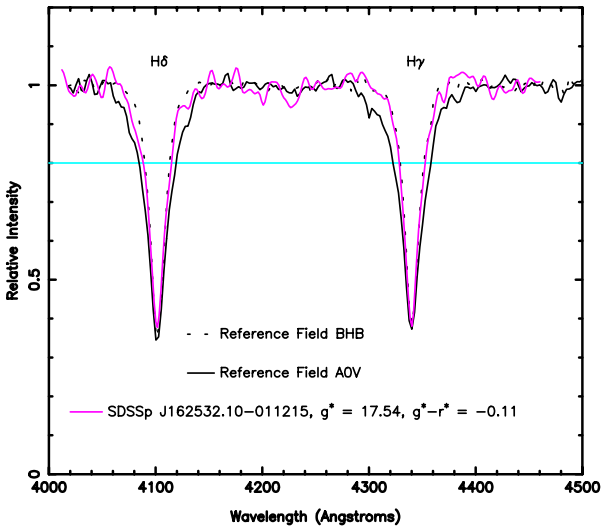
Hδ
Hγ
Relative Intensity
Wavelength (Angstroms)
- - Reference Field BHB
Reference Field A0V
SDSSp J162532.10–011215, g* = 17.54, g*–r* = –0.11

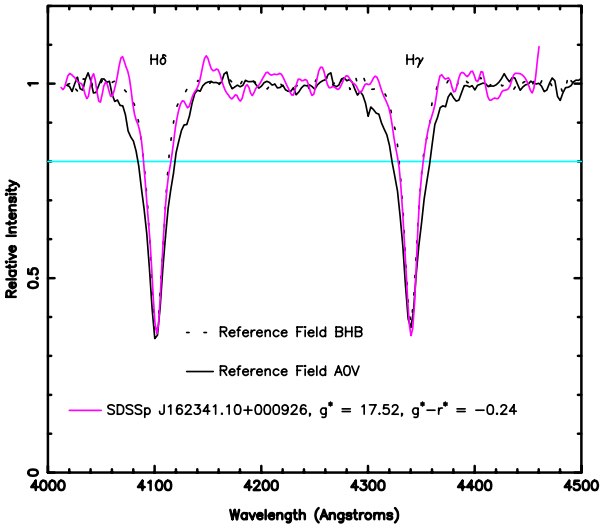
Hδ
Hγ
Relative Intensity
Wavelength (Angstroms)
- - Reference Field BHB
Reference Field A0V
SDSSp J162341.10+000926, g* = 17.52, g*–r* = –0.24

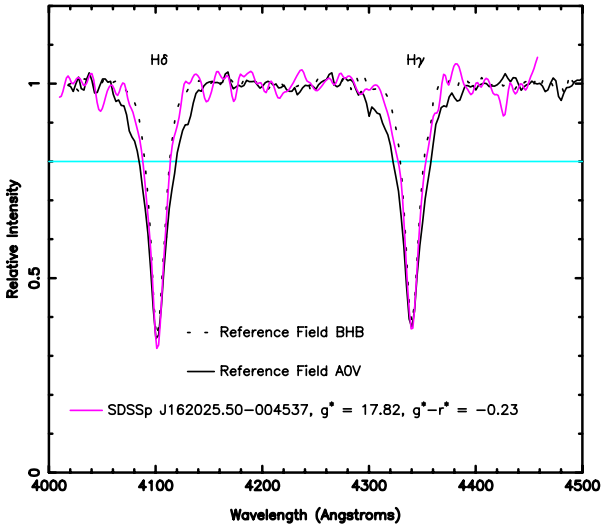
Hδ
Hγ
Relative Intensity
Wavelength (Angstroms)
- - Reference Field BHB
Reference Field A0V
SDSSp J162025.50–004537, g* = 17.82, g*–r* = –0.23

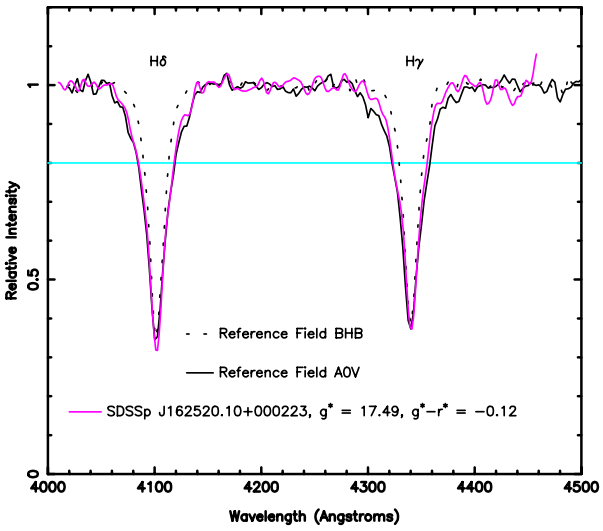
Hδ
Hγ
Relative Intensity
Wavelength (Angstroms)
- - Reference Field BHB
Reference Field A0V
SDSSp J162520.10+000223, g* = 17.49, g*–r* = –0.12

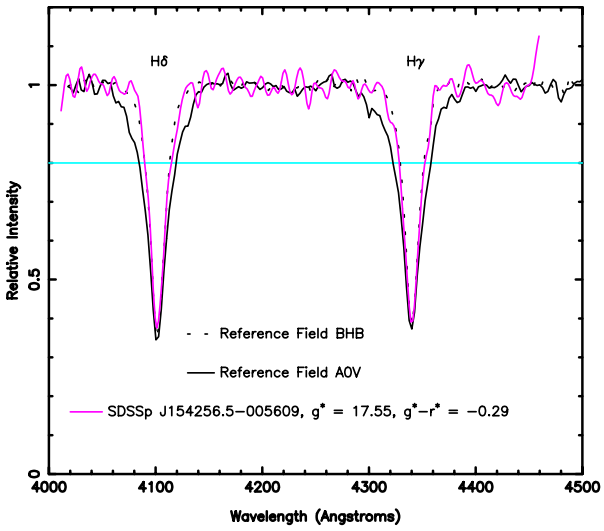
Hδ
Hγ
Relative Intensity
Wavelength (Angstroms)
- - Reference Field BHB
Reference Field A0V
SDSSp J154256.5–005609, g* = 17.55, g*–r* = –0.29

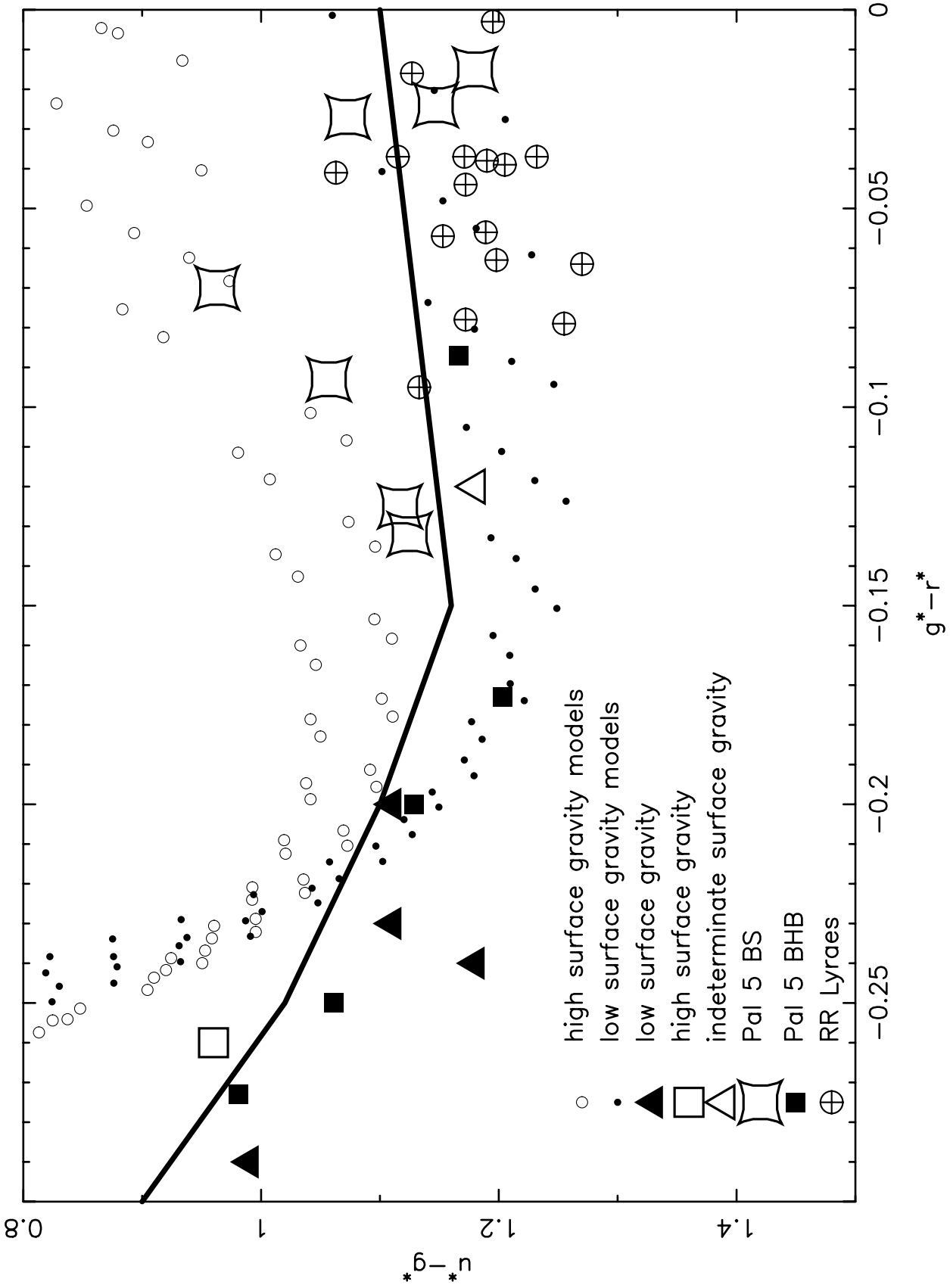
high surface gravity models
low surface gravity models
low surface gravity
high surface gravity
indeterminate surface gravity
Pal 5 BS
Pal 5 BHB
RR Lyrae
u*−g*
g*−r*
0.8
1
1.2
1.4
−0.25
−0.2
−0.15
−0.1
−0.05
0

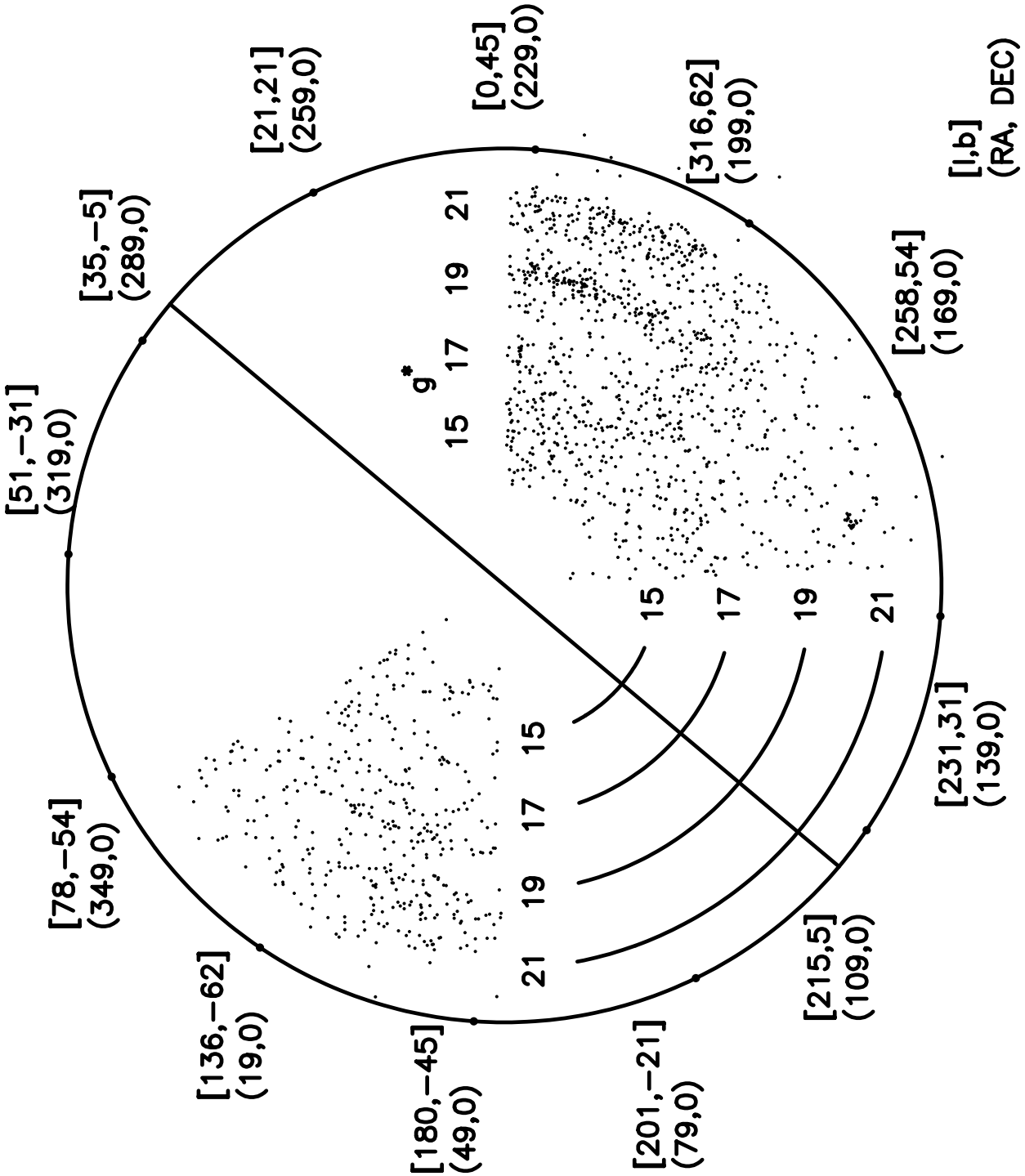
[0,45]
(229,0)
[21,21]
(259,0)
[35,−5]
(289,0)
[51,−31]
(319,0)
[78,−54]
(349,0)
[136,−62]
(19,0)
[180,−45]
(49,0)
[201,−21]
(79,0)
[215,5]
(109,0)
[231,31]
(139,0)
[258,54]
(169,0)
[316,62]
(199,0)
[l,b]
(RA, DEC)
g*
15
17
19
21

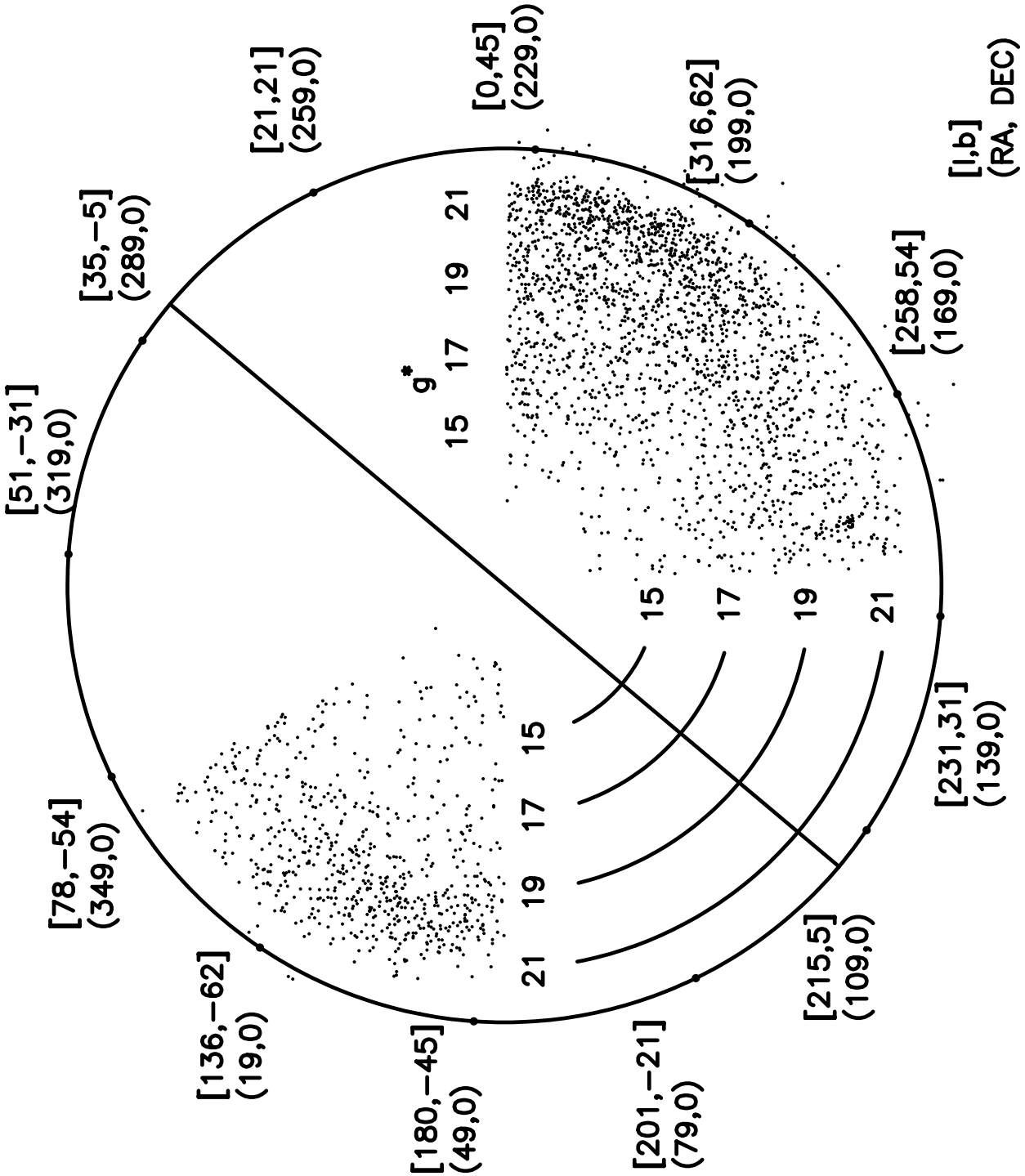
[0,45]
(229,0)
[21,21]
(259,0)
[35,−5]
(289,0)
[51,−31]
(319,0)
[78,−54]
(349,0)
[136,−62]
(19,0)
[180,−45]
(49,0)
[201,−21]
(79,0)
[215,5]
(109,0)
[231,31]
(139,0)
[258,54]
(169,0)
[316,62]
(199,0)
[l,b]
(RA, DEC)
g*
15
17
19
21

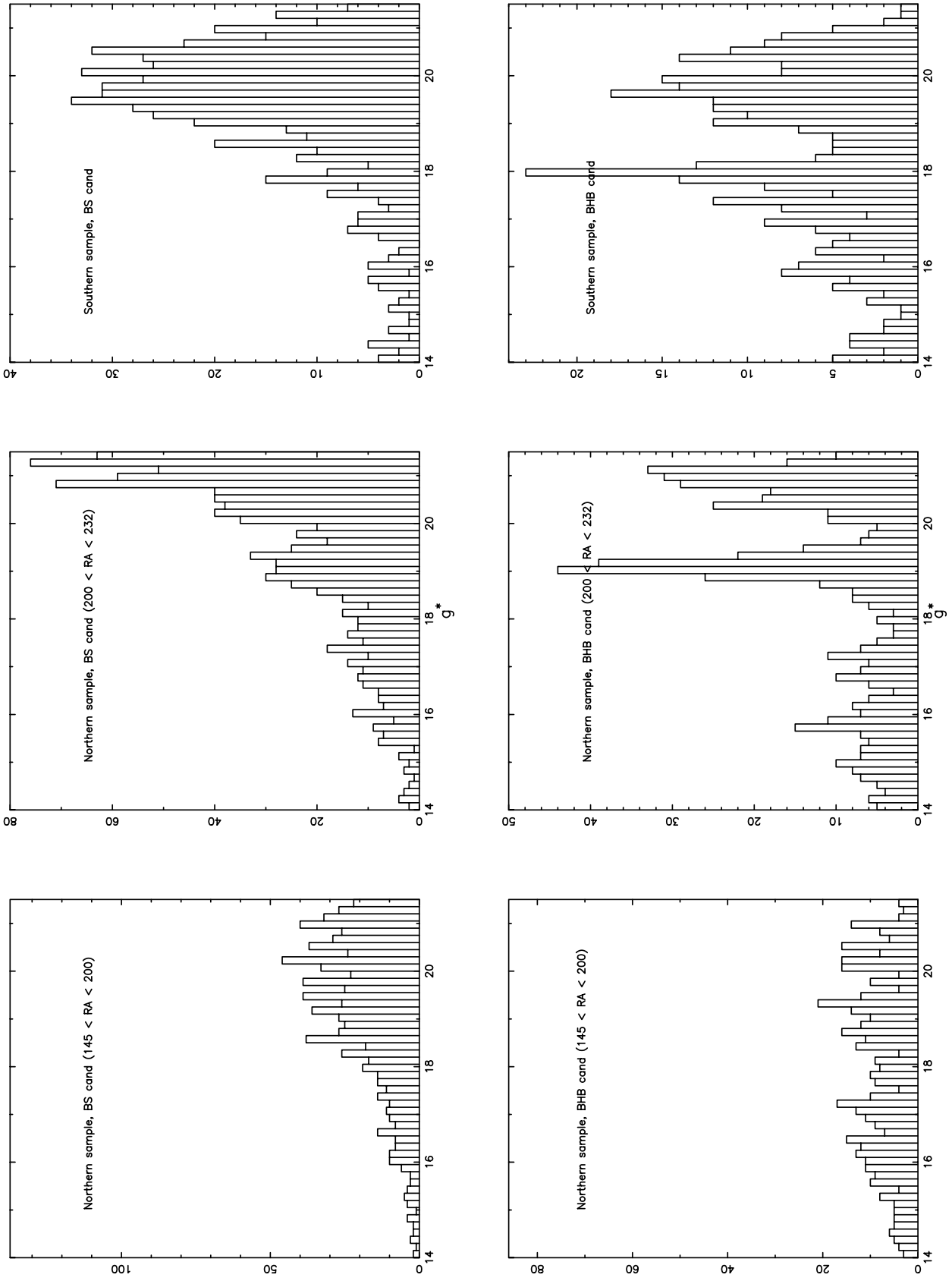
Southern sample, BS cand
Southern sample, BHB cand
Northern sample, BS cand (200 < RA < 232)
Northern sample, BHB cand (200 < RA < 232)
Northern sample, BS cand (145 < RA < 200)
Northern sample, BHB cand (145 < RA < 200)
g*

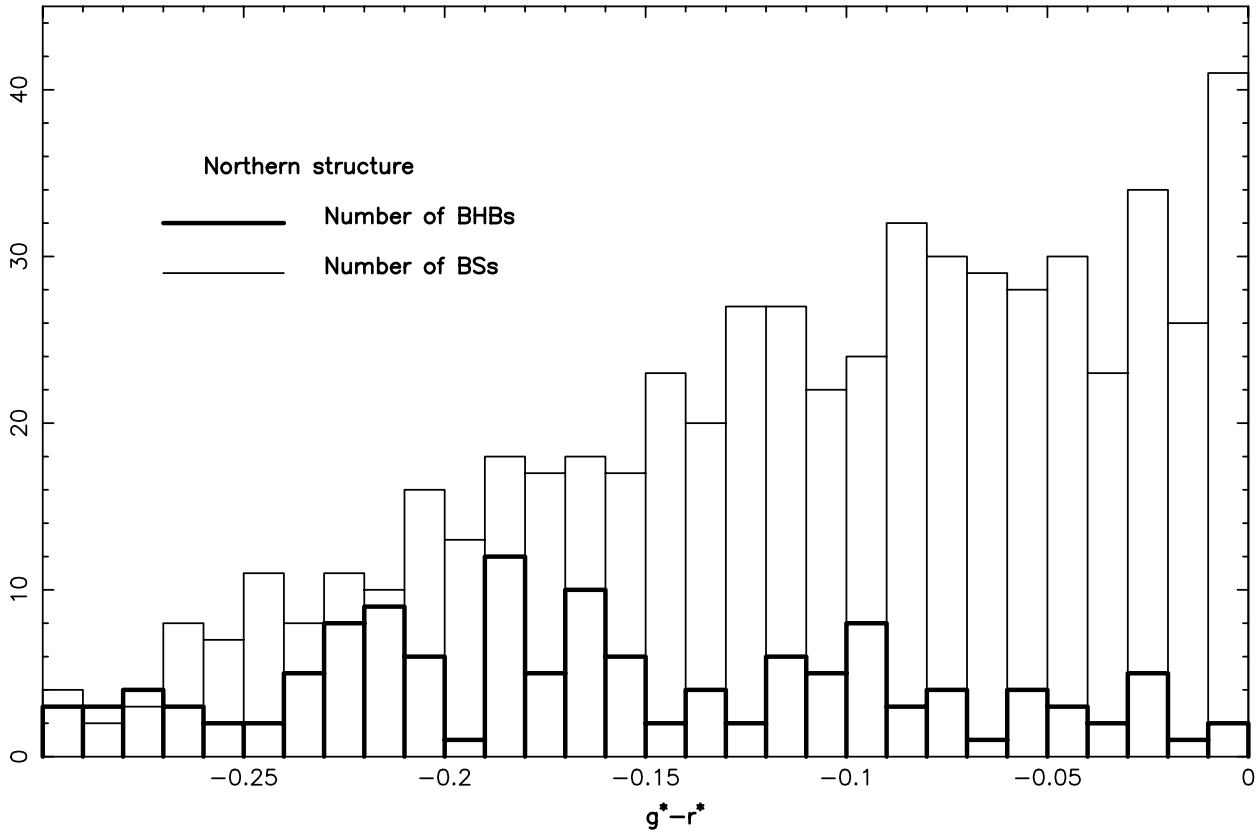
Northern structure
Number of BHBs
Number of BSs
0
10
20
30
40
−0.25
−0.2
−0.15
−0.1
−0.05
0
g*−r*

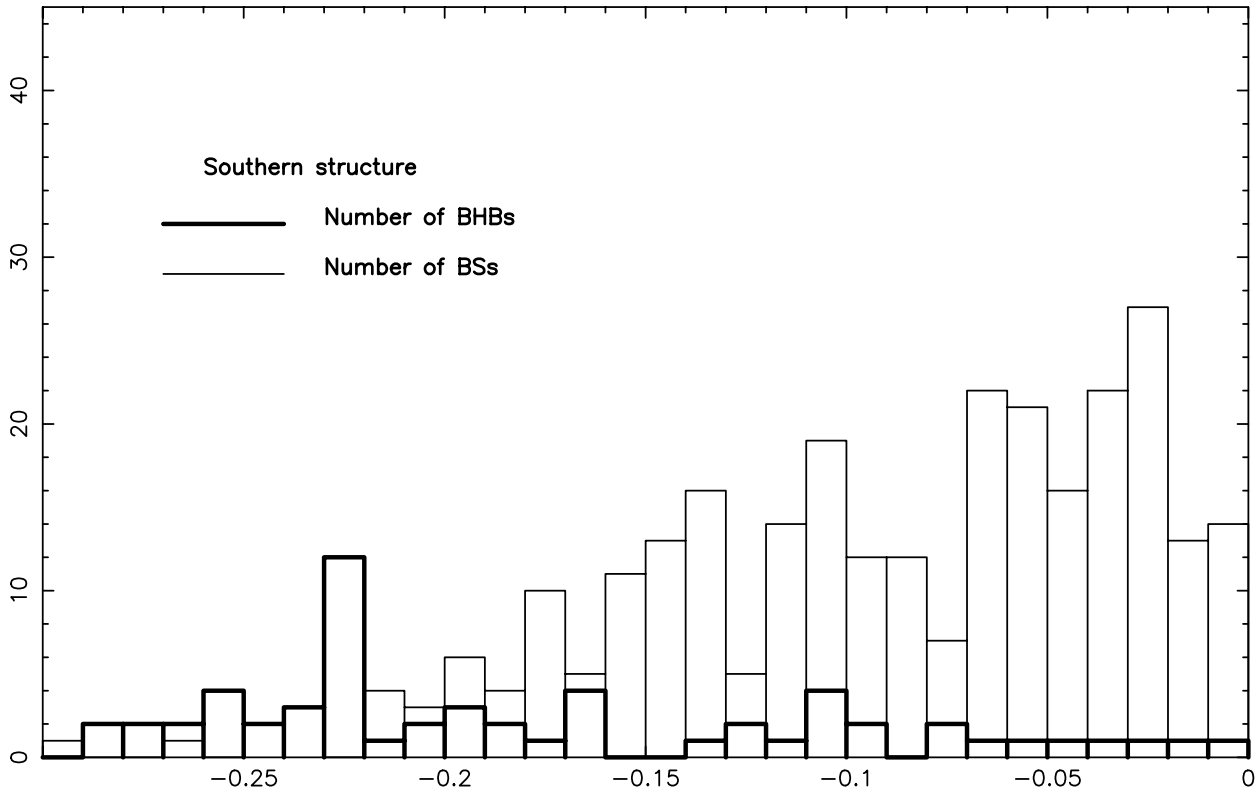
Southern structure
Number of BHBs
Number of BSs
0
10
20
30
40
−0.25
−0.2
−0.15
−0.1
−0.05
0

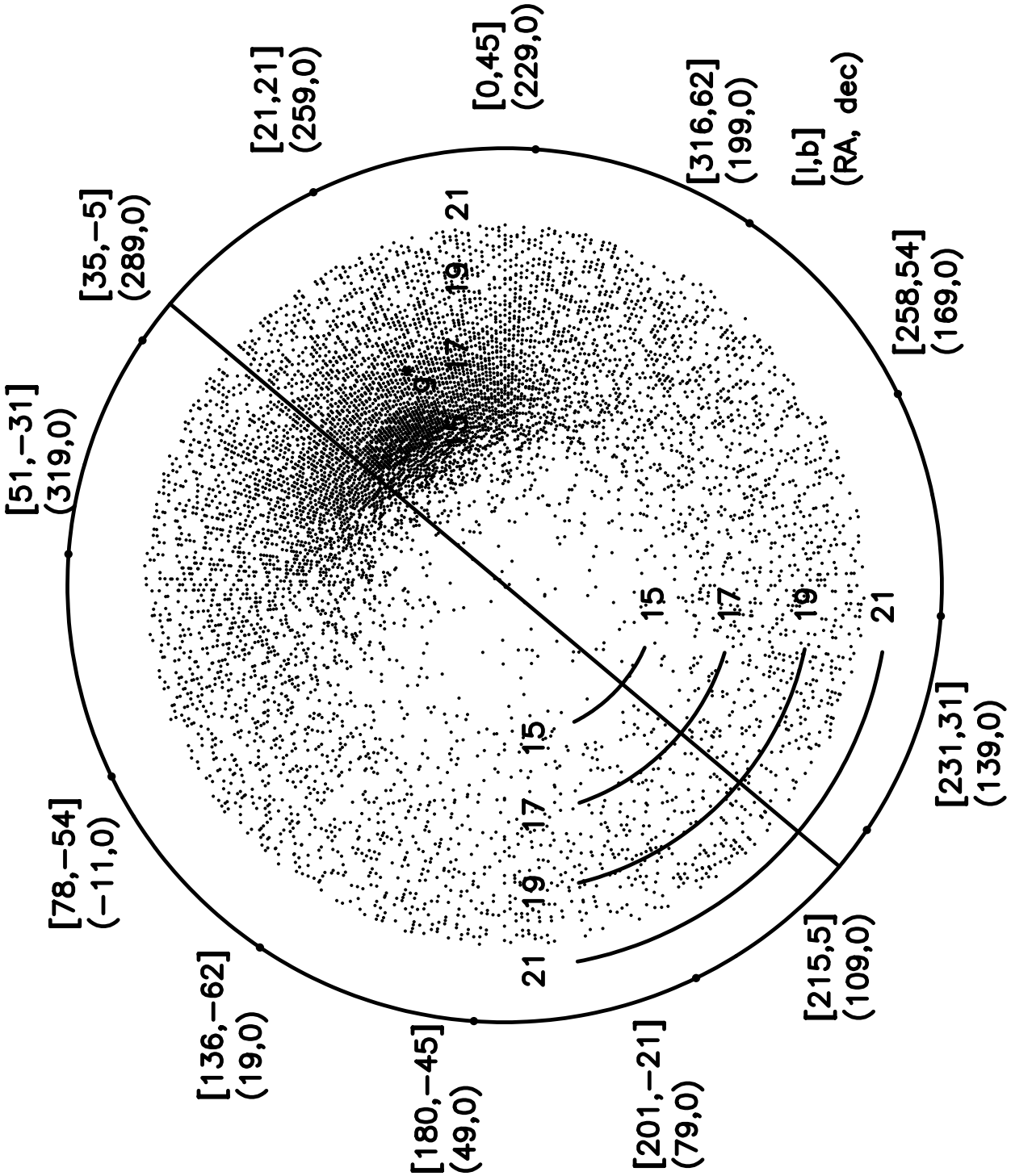
[0,45]
(229,0)
[21,21]
(259,0)
[35,−5]
(289,0)
[51,−31]
(319,0)
[78,−54]
(−11,0)
[136,−62]
(19,0)
[180,−45]
(49,0)
[201,−21]
(79,0)
[215,5]
(109,0)
[231,31]
(139,0)
[258,54]
(169,0)
[316,62]
(199,0)
[l,b]
(RA, dec)
15
17
19
21

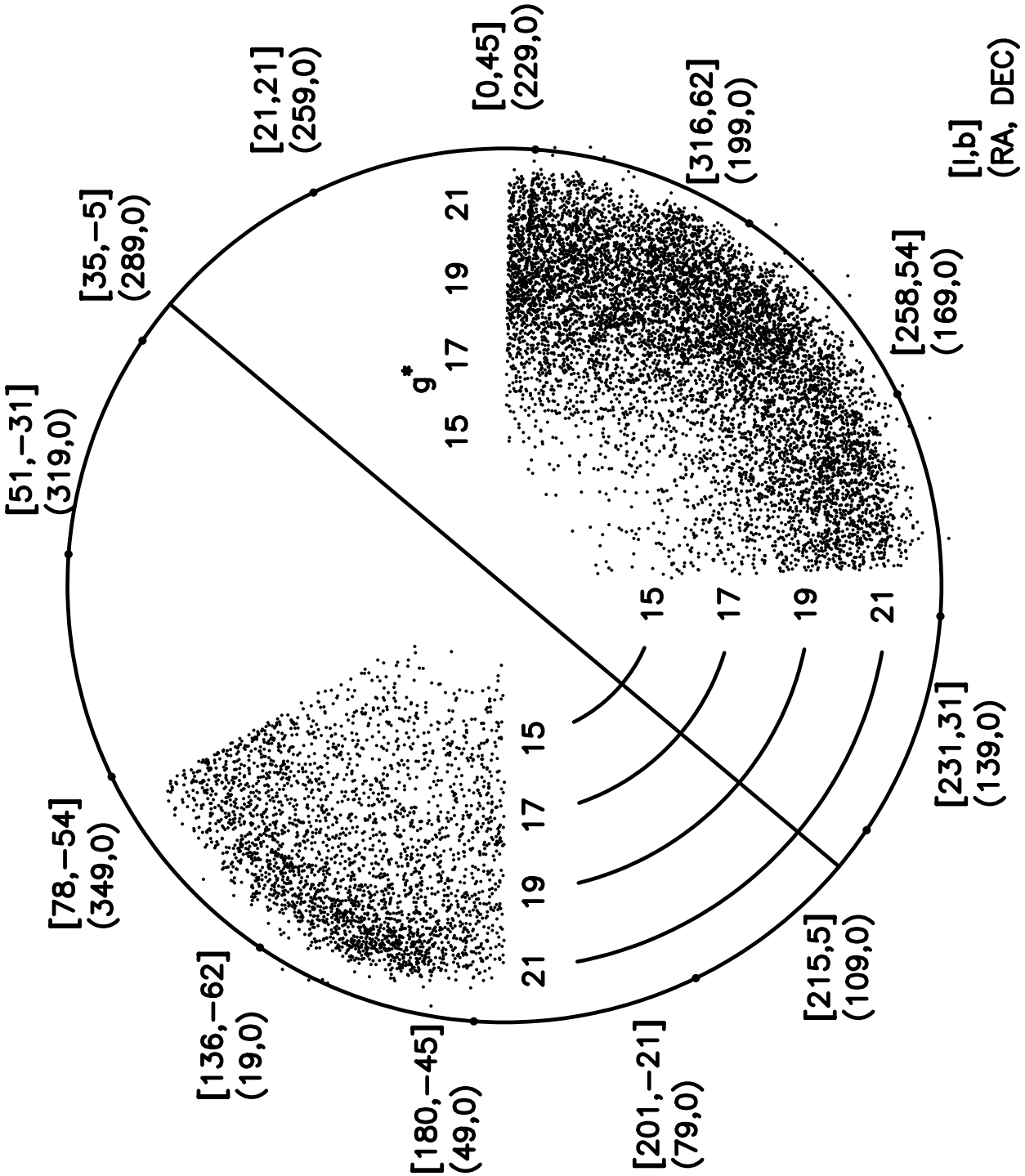
[0,45]
(229,0)
[21,21]
(259,0)
[35,−5]
(289,0)
[51,−31]
(319,0)
[78,−54]
(349,0)
[136,−62]
(19,0)
[180,−45]
(49,0)
[201,−21]
(79,0)
[215,5]
(109,0)
[231,31]
(139,0)
[258,54]
(169,0)
[316,62]
(199,0)
[l,b]
(RA, DEC)
g*
15
17
19
21

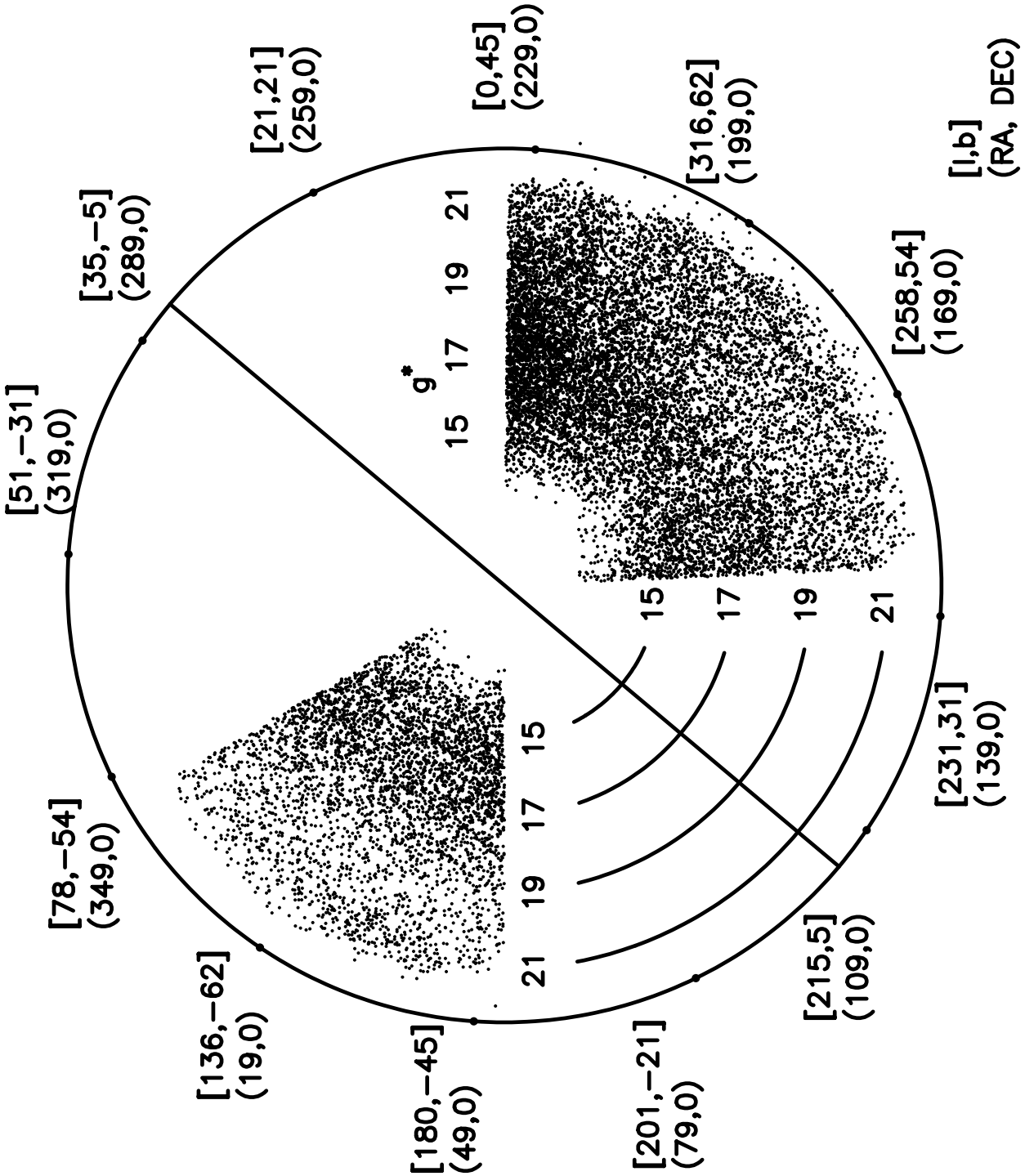
[l,b]
(RA, DEC)
[0,45]
(229,0)
[21,21]
(259,0)
[35,−5]
(289,0)
[51,−31]
(319,0)
[78,−54]
(349,0)
[136,−62]
(19,0)
[180,−45]
(49,0)
[201,−21]
(79,0)
[215,5]
(109,0)
[231,31]
(139,0)
[258,54]
(169,0)
[316,62]
(199,0)
g*
15
17
19
21

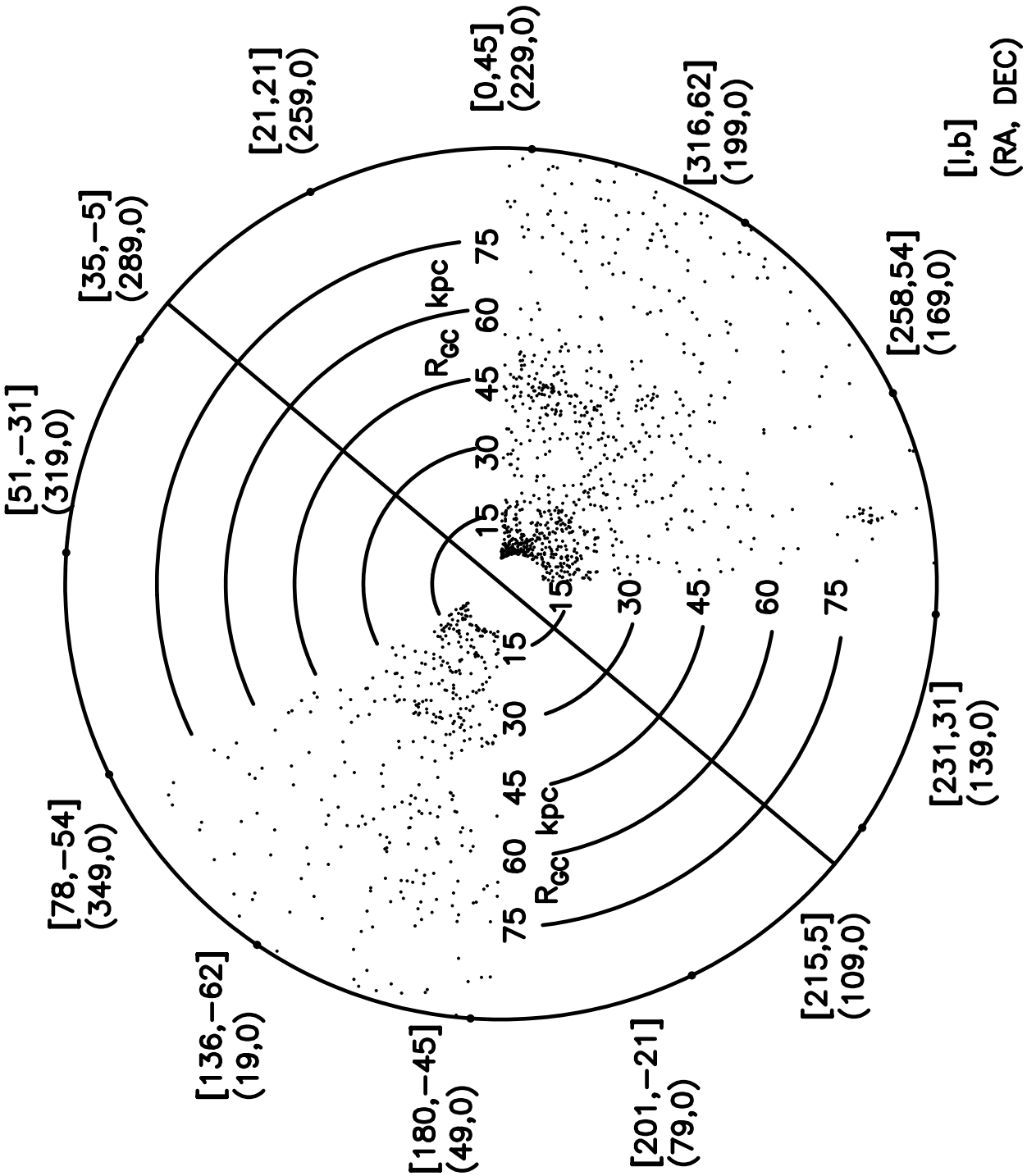
[0,45]
(229,0)
[21,21]
(259,0)
[35,−5]
(289,0)
[51,−31]
(319,0)
[78,−54]
(349,0)
[136,−62]
(19,0)
[180,−45]
(49,0)
[201,−21]
(79,0)
[215,5]
(109,0)
[231,31]
(139,0)
[258,54]
(169,0)
[316,62]
(199,0)
[l,b]
(RA, DEC)
R_GC kpc
15
30
45
60
75

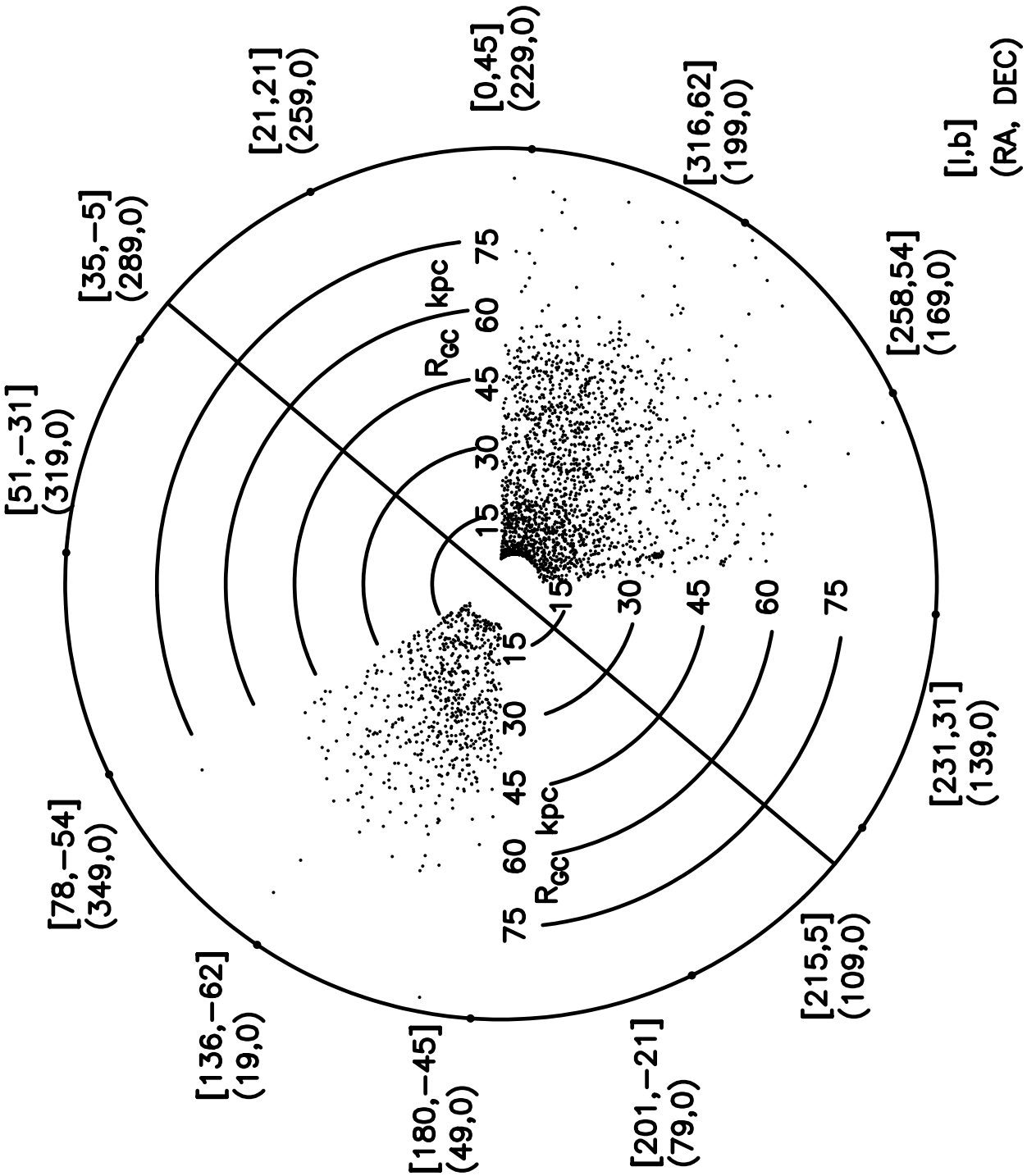
[0,45]
(229,0)
[21,21]
(259,0)
[35,−5]
(289,0)
[51,−31]
(319,0)
[78,−54]
(349,0)
[136,−62]
(19,0)
[180,−45]
(49,0)
[201,−21]
(79,0)
[215,5]
(109,0)
[231,31]
(139,0)
[258,54]
(169,0)
[316,62]
(199,0)
[l,b]
(RA, DEC)
R_GC kpc
15
30
45
60
75

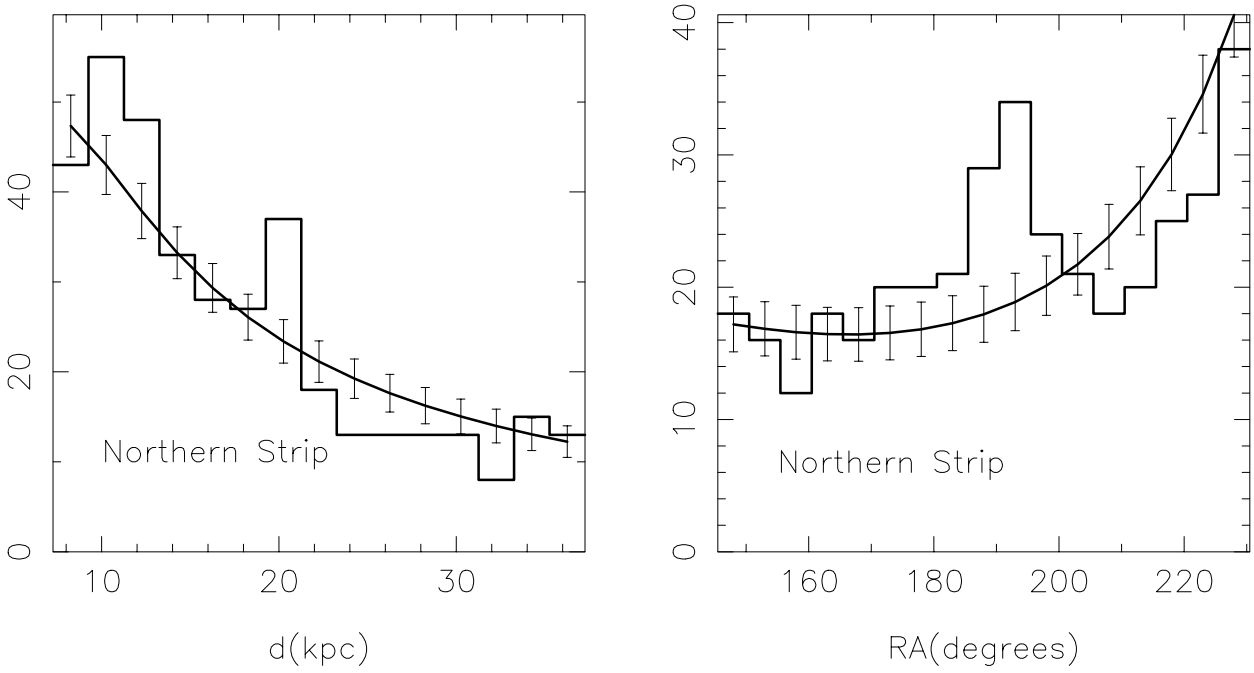
Northern Strip
d(kpc)
Northern Strip
RA(degrees)

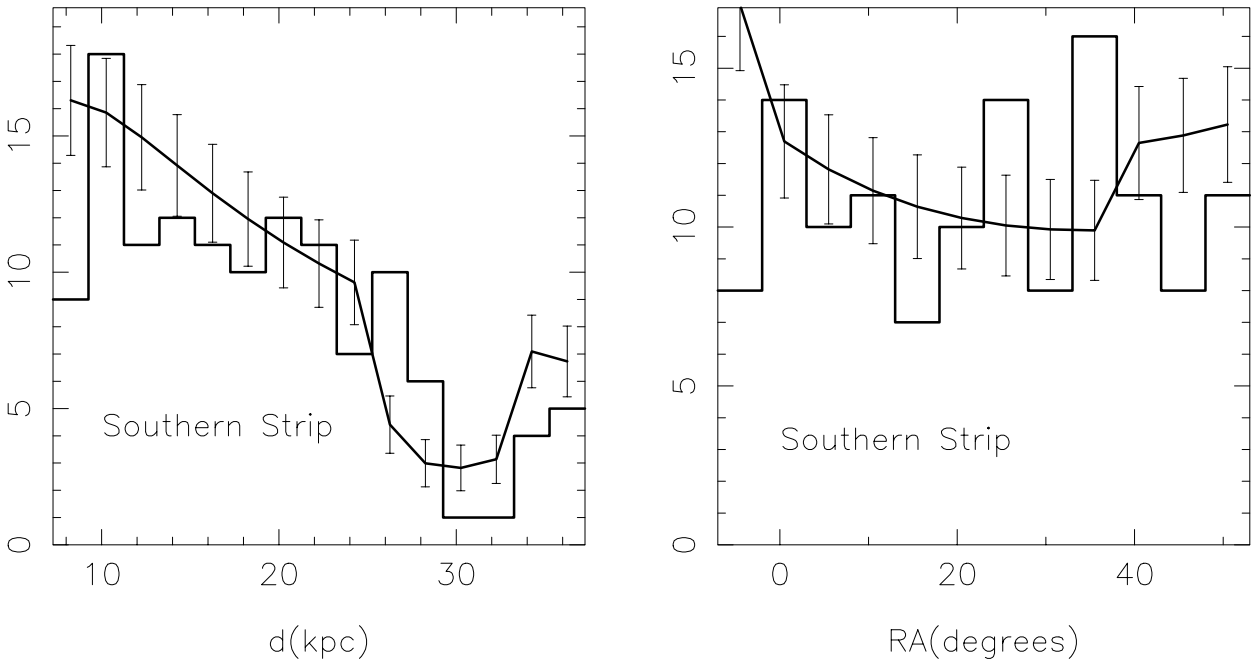
Southern Strip
d(kpc)
Southern Strip
RA(degrees)